Computer Methods in Biomechanics and Biomedical Engineering, Vol. 3, pp. 1–30
Reprints available directly from the publisher
Photocopying permitted by license only

The Obstacle-Set Method for Representing Muscle Paths in Musculoskeletal Models

BRIAN A. GARNER and MARCUS G. PANDY*

Department of Mechanical Engineering and Department of Kinesiology, University of Texas at Austin, Austin, Texas 78712, U.S.A.

(Received 17 March 1998; In final form 25 February 1999)

A computational method is introduced for modeling the paths of muscles in the human body. The method is based on the premise that the resultant muscle force acts along the locus of the transverse cross-sectional centroids of the muscle. The path of the muscle is calculated by idealizing its centroid path as a frictionless elastic band, which moves freely over neighboring anatomical constraints such as bones and other muscles. The anatomical constraints, referred to as obstacles, are represented in the model by regular-shaped, rigid bodies such as spheres and cylinders. The obstacles, together with the muscle path, define an obstacle set. It is proposed that the path of any muscle can be modeled using one or more of the following four obstacle sets: single sphere, single cylinder, double cylinder, and sphere-capped cylinder. Assuming that the locus of the muscle centroids is known for an arbitrary joint configuration, the obstacle-set method can be used to calculate the path of the muscle for all other joint configurations. The obstacle-set method accounts not only for the interaction between a muscle and a neighboring anatomical constraint, but also for the way in which this interaction changes with joint configuration. Consequently, it is the only feasible method for representing the paths of muscles which cross joints with multiple degrees of freedom such as the deltoid at the shoulder.

Keywords: Muscle paths, moment arms, musculoskeletal geometry

INTRODUCTION

Mathematical models are commonly used to determine the forces transmitted by the muscles, ligaments, and articular surfaces at the joints during movement [1–14]. The results of these studies are sensitive to the model assumed for the muscle paths because, for a given configuration of the joints, the paths of the muscles determine the lengths, moment arms, forces, and torques of the muscles at the joints [15,16].

Two distinctly different models have been used to represent the paths of muscles in the body: the straight-line model and the centroid-line model. In the straight-line model, the path of the muscle is represented by a straight line joining the centroids of

*Corresponding author.

the muscle attachment areas [1,5,17–20]. Although this model is relatively easy to implement, it may not yield meaningful results when the muscle passes through a tendon sheath or when it wraps around a bone or another muscle. Alternatively, the centroid-line model represents the path of the muscle by a line that passes through the locus of cross-sectional centroids of the muscle [10,21–23]. Although the centroid-line model produces a more realistic description of the muscle's line of action, application of this model is limited by the fact that the locations of the muscle cross-sectional centroids are difficult to obtain for even a single configuration of the joint [21,24–26]. Furthermore, even if the muscle centroid path is known for one joint configuration, the problem remains to represent the path of the muscle for all other configurations of the joint.

Several approaches have been used to approximate the centroid-line path of a muscle for all joint configurations. One method is to introduce effective attachment sites, or via points, at specific locations along the centroid path, and to assume that the line of action of the muscle is defined either by straight-line segments or by a combination of straight-line and curved-line segments between the via points [20,27–31]. In either case, the via points remain fixed relative to the bones even as the joints move. To account for anatomical constraints, such as when the muscle wraps over a bone or another muscle, these via points become active or inactive depending on the joint configuration. Although this approach is reasonable when representing the path of a muscle spanning a simple revolute joint, it is generally not adequate for joints which have more than one rotational degree of freedom. Joint motion occurring in more than one plane can cause the muscle path to slide over the surfaces of the anatomical constraints, and importantly, the fixed-via-point method does not account for such effects. This method may therefore produce discontinuities in the length and moment arm of the muscle at joint configurations where via points become active or inactive.

In this paper, an alternate approach is presented for modeling the path of a muscle for all joint configurations. This approach, the *obstacle-set* method, is based on three assumptions. First, the force transmitted by a muscle acts along the locus of the transverse cross-sectional centroids of the muscle [21]. Second, the centroid path of the muscle can be idealized as a frictionless elastic band that moves freely over neighboring anatomical constraints [32,33]. Third, anatomical structures that constrain the path of the muscle may be represented by regular-shaped, rigid bodies such as spheres and cylinders. If the locus of the muscle centroids is known for an arbitrary joint configuration, an obstacle-set model may be constructed for the muscle path, and, by applying the algorithms presented in this paper, the path of the muscle can be calculated for all other configurations of the joint.

OBSTACLE-SET TERMINOLOGY

In the obstacle-set method, a muscle path is defined by a series of straight-line and curved-line segments joined together by via points. These via points may or may not be fixed relative to the bones. Straight-line segments span adjacent via points unencumbered, whereas curved-line segments wrap around anatomical structures which constrain the path of the muscle. An *obstacle* is a regular-shaped rigid body that is used to model the shape of a constraining anatomical structure; typical examples of muscle-path constraints are bones and other muscles (see Figure 1). A reference frame is any set of three orthogonal unit vectors that is fixed on a rigid body and is used to specify the position and orientation of the body in space. *Bone reference frames* are attached to bones, and *obstacle reference frames* are attached to obstacles. A *via point* is a point along a muscle path whose position is constrained by the presence of another anatomical structure. A via point may be *active* (the muscle path passes through the point) or *inactive* (the muscle path does not pass through the point). There are two types of via points: a *fixed via point* remains fixed in a bone reference frame and is always active; an *obstacle via point* is not fixed in any reference frame, but is constrained to move on the surface of an underlying obstacle.

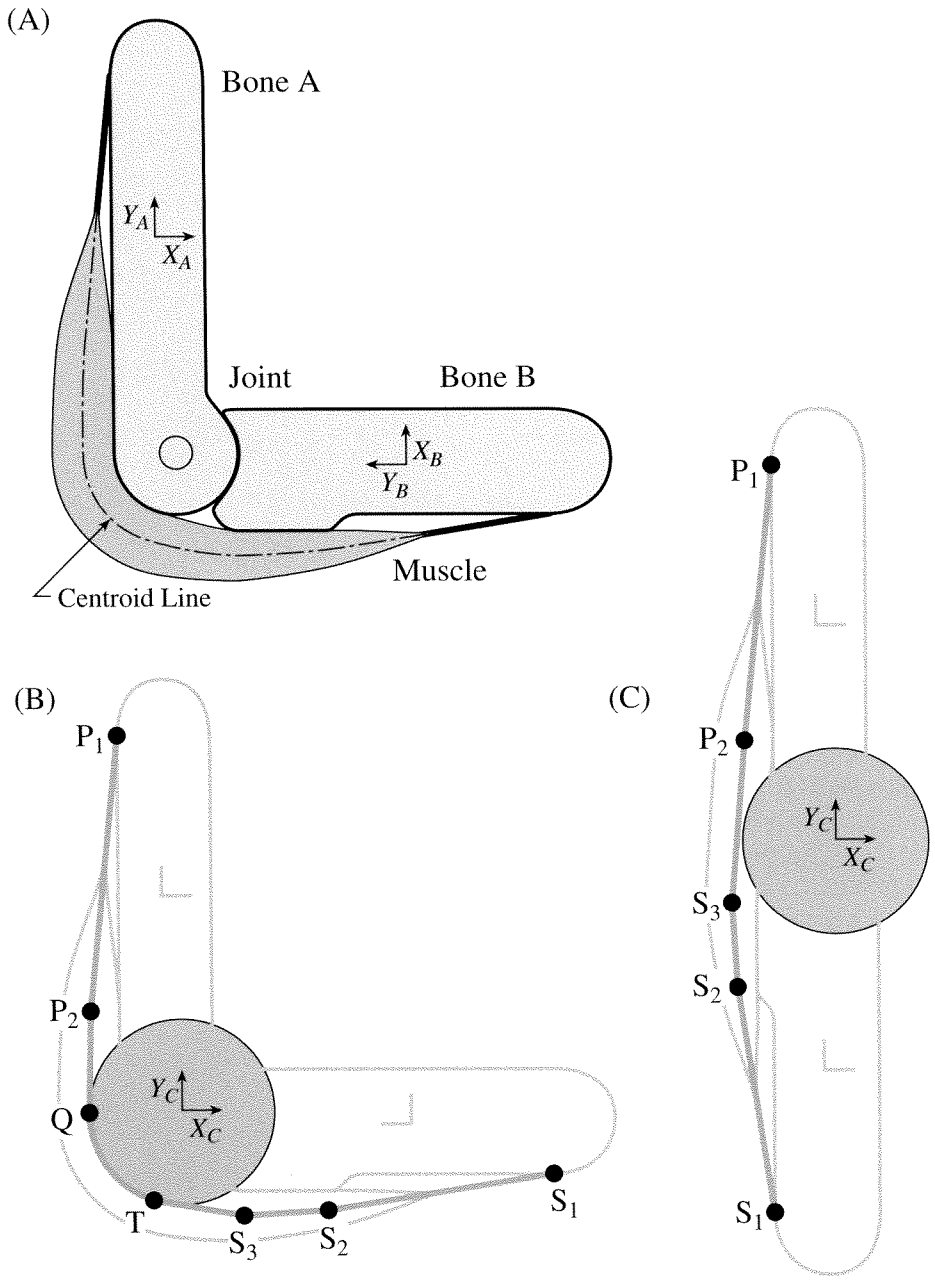

FIGURE 1 Schematic of a hypothetical muscle (A) represented by the obstacle-set model (B and C). The muscle spans a single joint which connects bones A and B. Reference frames attached to the bones are used to describe the position and orientation of the bones relative to each other. At certain joint configurations, the muscle contacts the bones and causes the centroid path of the muscle to deviate from a straight line (A). The muscle path is modeled using a total of seven via points: five of these serve as fixed via points (***P1***, ***P2***, ***S1***, ***S2***, and ***S3***); the remaining two are obstacle via points (***Q*** and ***T***) which move relative to the bones and the obstacle. Points ***P1*** and ***S1*** are the origin and insertion of the muscle. Points ***P2*** and ***S3*** are bounding-fixed via points. The obstacle is shown as a shaded circle which represents the cross-section of a sphere or a cylinder. An obstacle reference frame positions and orients the obstacle relative to the bones. The obstacle is made larger than the cross sections of the bones in order to account for the thickness of the muscle belly. The obstacle set is defined by the obstacle, the four via points ***P2***, ***Q***, ***T***, and ***S3***, and the segments of the muscle path between the via points ***P2*** and ***S3***. At some joint configurations, the muscle path loses contact with the obstacle and the obstacle via points then become inactive (C).

An obstacle via point defines the beginning of contact with the obstacle and may become active or inactive as contact is made or lost. A fixed via point that lies adjacent to an obstacle via point in the path of the muscle is called a *bounding-fixed via point*. The portion of the muscle path that interacts with an obstacle is referred to as an *obstacle set*. An obstacle set usually comprises one obstacle, two bounding-fixed via points, two obstacle via points, and the path spanned by the muscle between the two bounding-fixed via points (Figure 1). It should be noted, however, that some obstacle sets do comprise more than one obstacle. Although there is no restriction on the number of obstacle sets which can be used to model the path of a muscle, in most cases a muscle's path may be accurately reproduced using a series of fixed via points and just one obstacle set. We propose that the path of any muscle can be modeled using one or more of the following obstacles sets: a single sphere, a single cylinder, a double cylinder, and a sphere-capped cylinder.

The single-sphere obstacle set is comprised of a sphere, two bounding-fixed via points, and two obstacle via points (Figure 2A). This obstacle set is most appropriate for modeling the paths of ligaments at a joint (e.g., the ACL when it contacts the roof of the intercondylar notch near full extension of the knee). Within the framework of the obstacle-set method, ligaments may be treated as passive muscles. The parameters which define the single-sphere obstacle set are the radius of the sphere, the position and orientation of a reference frame fixed at the center of the sphere, and the positions of the two bounding-fixed via points, each expressed in its own bone reference frame.

The single-cylinder obstacle set is comprised of a cylinder, two bounding-fixed via points, and two obstacle via points (Figure 2B). This obstacle set can be used to model the paths of uniarticular muscles which wrap around cylindrical structures such as long bones and the thorax. The parameters which define the single-cylinder obstacle set are the radius of the cylinder, the position and orientation of a reference frame fixed on the cylinder, and the positions of the two bounding-fixed via points, each expressed in its own bone reference frame.

The double-cylinder obstacle set is comprised of two cylinders, two bounding-fixed via points, and four obstacle via points, two for each cylinder (Figure 2C). This obstacle set can be used to model the path of biarticular muscles such as the long head of triceps brachii and the rectus femoris. There are no restrictions on either the size or the position and orientation of each cylinder used in the obstacle set, provided that the cylinders do not interfere with each other in the regions where the muscle path contacts the cylinders. The parameters which define the double-cylinder obstacle set are the radius of each cylinder, the position and orientation of the reference frame fixed on each cylinder, and the positions of the two bounding-fixed via points, each expressed in its own bone reference frame. The double-cylinder obstacle set differs from two consecutive single-cylinder obstacle sets in that no bounding-fixed via point appears between the cylinders. Therefore, the positions of the obstacle via points in the double-cylinder obstacle set are not independent (see Appendix E).

The most complicated of the proposed obstacle sets is the sphere-capped cylinder. This obstacle set is comprised of a single sphere, a single cylinder, two bounding-fixed via points, and three obstacle via points (Figure 2D). The sphere and cylinder share a common radius, with the center of the sphere lying on the axis of the cylinder. The sphere-capped cylinder was designed to model the paths of relatively long muscles which span joints with more than one rotational degree of freedom (e.g., the three heads of deltoid at the shoulder). The parameters which define the sphere-capped obstacle set are the radius of the sphere (which is equal to the radius of the cylinder), the position and orientation of a reference frame fixed at the center of the sphere, and the positions of the two bounding-fixed via points, each expressed in its own bone reference frame.

OBSTACLE-SET ALGORITHM

The obstacle-set algorithm assumes that the skeleton is modeled as a set of rigid bodies (bones) which

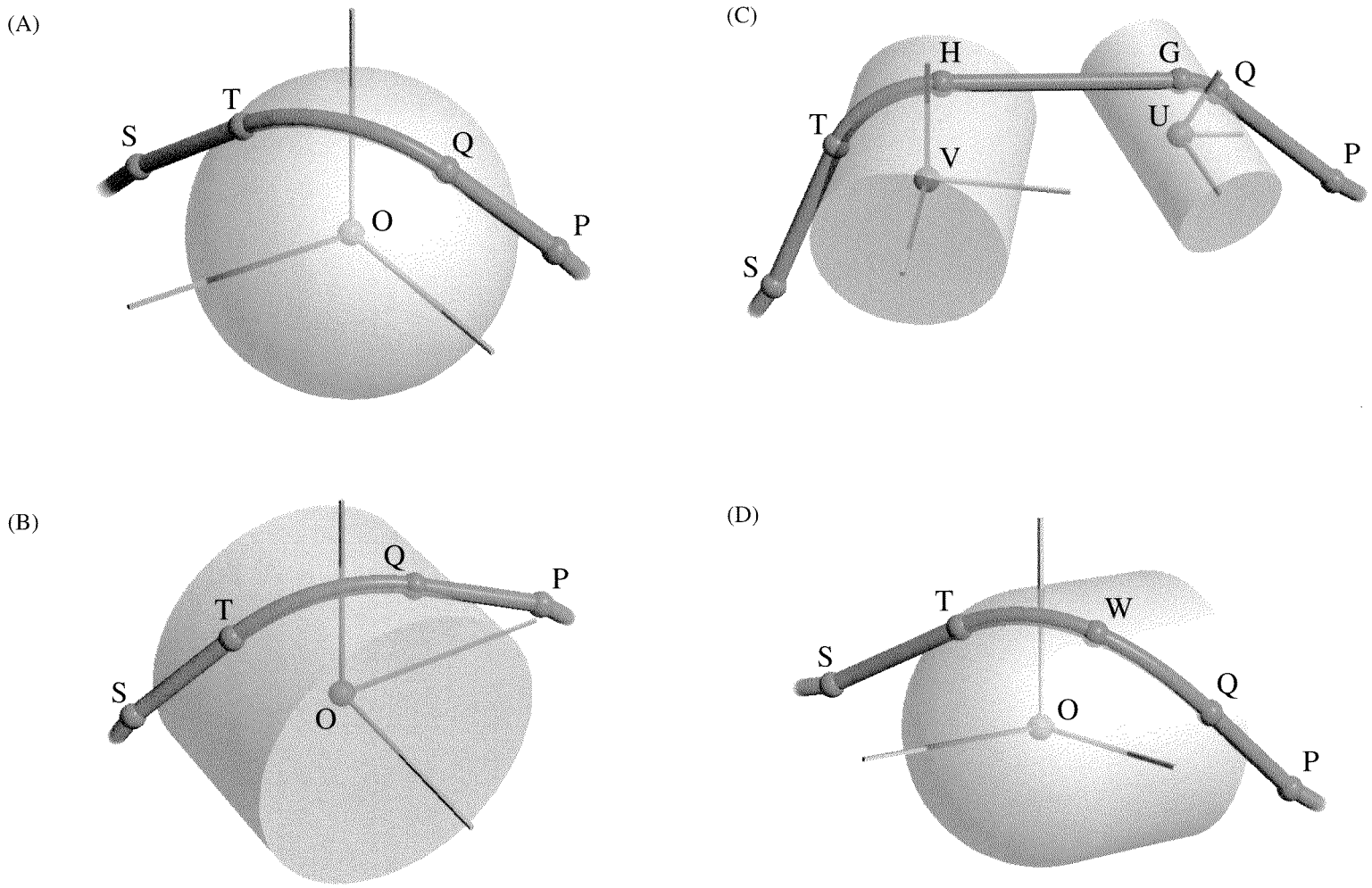

FIGURE 2 Graphical representation of each of the four obstacle sets: (A) single sphere, (B) single cylinder, (C) double cylinder, and (D) sphere-capped cylinder. Each obstacle set comprises a portion of the muscle path, one or more obstacles, two bounding-fixed via points, and two or more obstacle via points. A reference frame attached to each obstacle defines the position and orientation of the obstacle relative to the neighboring bones. Whenever possible, the reference frame is aligned with the geometry of the obstacle in order to simplify the mathematical equations in the obstacle-set algorithm. Symbols appearing in the diagram are defined in the Appendices, which describe the obstacle sets in detail.

articulate at well-defined joints. For a given configuration of the joints, the skeletal model fully describes the relative positions and orientations of the bones. Furthermore, since obstacles and fixed via points are fixed relative to the bones, the positions and orientations of these objects are also known for a given configuration of the joints. The problem, then, is to calculate the unknown positions of the obstacle via points within the muscle path. Since the muscle is idealized as a frictionless elastic band, the path of the muscle is determined by minimum potential energy. Thus, the problem is equivalent to finding the minimum-distance path between the two bounding-fixed via points within an obstacle set. Consider again the muscle path shown in Figure 1. The model for the muscle path is constrained by a single obstacle, which is fixed to bone A (Figures, 1B and C). The path of the muscle is defined by the positions of the five fixed via points and the positions of the two obstacle via points. Via points $\boldsymbol{P_1}$ and $\boldsymbol{P_2}$ are fixed to bone A, whereas via points $\boldsymbol{S_1}$, $\boldsymbol{S_2}$, and $\boldsymbol{S_3}$ are fixed to bone B. For a given configuration of the joint, the paths of all segments of the muscle are known, except those between the bounding-fixed via points, $\boldsymbol{P_2}$ and $\boldsymbol{S_3}$. Calculating the positions of the obstacle via points, $\boldsymbol{Q}$ and $\boldsymbol{T}$, then fully describes the muscle path.

There are four steps in the computational algorithm that is used to find the locations of the obstacle via points for a specific obstacle set at a given joint configuration (Figure 3). First, the positions of the two bounding-fixed via points are expressed in the obstacle reference frame. Second, the locations of the obstacle via points are found assuming that these points are all active. Third, a wrapping condition is used to determine which, if any, of the obstacle via points are inactive (see Appendix A). If any of the obstacle via points are found to be inactive, steps 2 and 3 are repeated with the inactive via points removed from the calculation of the muscle path. Fourth, the locations of all active via points are used to calculate the length of each muscle segment between the two bounding-fixed via points. Since the geometry of each obstacle set shown in Figure 2 is different, a separate version of the computational algorithm given in Figure 3 was developed for each obstacle set (see Appendices C through F).

APPLICATION TO THE UPPER LIMB

The algorithms given in the Appendices were used to model the paths of the triceps brachii and deltoid muscles in the arm. The paths of these muscles were calculated using a kinematic model of the arm, which was developed from high-resolution medical images obtained from the National Library of Medicine's Visible Human Male (VHM) dataset [34]. The kinematic model includes seven joints and uses thirteen degrees of freedom to describe the relative movements of seven upper-extremity bones: the clavicle, scapula, humerus, ulna, radius, carpal bones, and hand. Locations of the joint centers and joint axes were derived directly from three-dimensional bone surfaces, which were reconstructed from the medical images. The centroid path of each muscle was calculated from transverse cross sections of reconstructed muscle surfaces (also reconstructed from the medical images) taken over the whole length of the muscle belly. To evaluate the accuracy with which the obstacle-set model is able to represent the path of each muscle, we compared the moment arms calculated from the model with measured values obtained from human cadavers [35,36]. In the model, as in the experiments, the moment arm of each muscle was found by calculating muscle length over the full range of joint movement, and by then computing the derivative of muscle length with respect to joint angle [37–39].

Triceps Brachii

The triceps brachii is a large, thick muscle which is divided into three parts: the long head, the medial head, and the lateral head. The long head, which originates from a depression on the scapula that is immediately below the glenoid cavity, spans both the glenohumeral and elbow joints. The medial and lateral heads, which originate from the posterior surface of the shaft of the humerus, span only

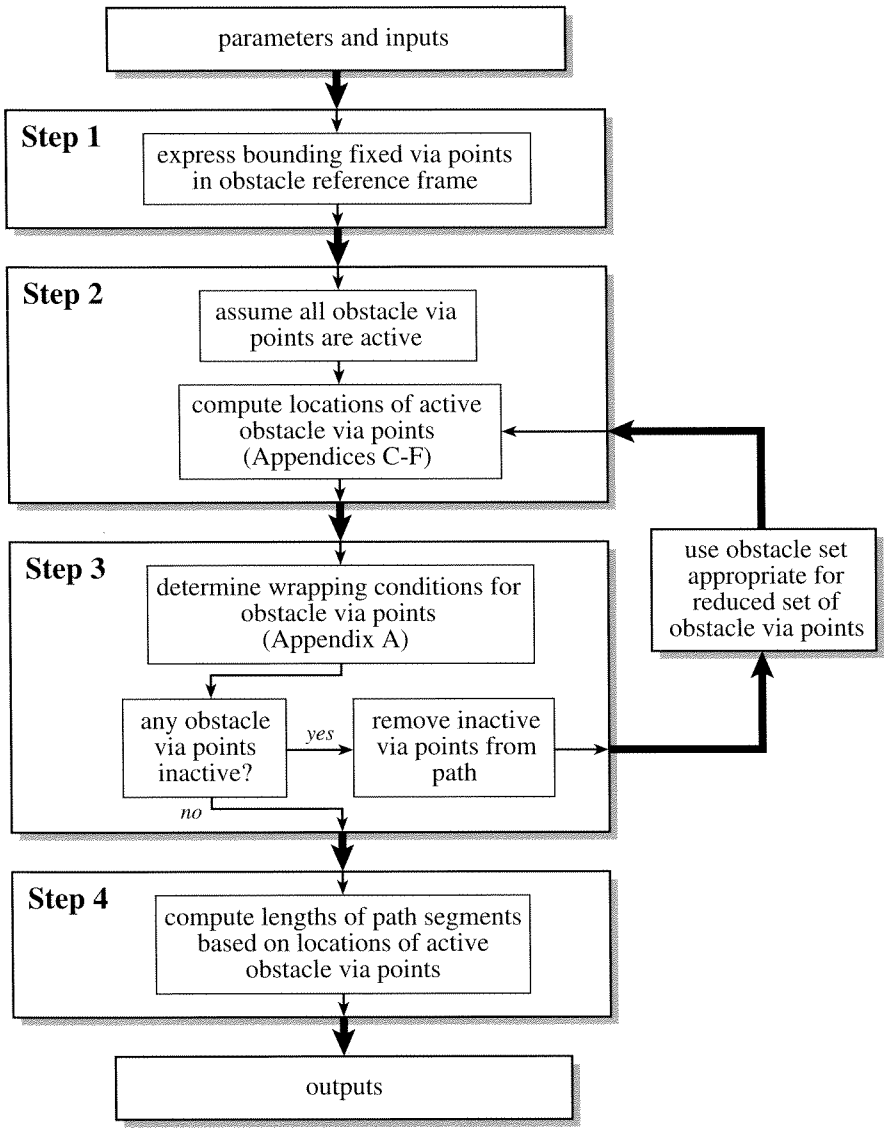

FIGURE 3 Flowchart of the obstacle-set algorithm. The purpose of the algorithm is to completely describe the centroid path of a muscle for a given configuration of the joints. Given the relative positions of the bones, the locations of all fixed via points are known and may be expressed in the obstacle reference frame (Step 1). The locations of the remaining via points in the muscle path, the obstacle via points, may be calculated using one or more of the four different types of obstacle sets described in this paper (Step 2). A separate version of the obstacle-set algorithm for each of the four different obstacle sets is given in Appendices C-F. Once the locations of the obstacle via points are known, a check is made to determine whether any of these points should be inactive (Step 3). If an obstacle via point should be inactive, it is removed from the muscle path and the locations of the remaining obstacle via points are then recomputed (repeat Steps 2 and 3). Finally, the lengths of the muscle-path segments between all of the active via points are computed (Step 4).

the elbow. All three heads insert on the olecranon process of the ulna, and so they wrap around the distal humerus as the elbow is moved into flexion.

Each head of the triceps brachii was represented as a separate and distinct muscle path with its own obstacle set. The origin and insertion of each path were found by inspecting transverse cross-sections of the muscle obtained from the VHM dataset and by calculating the centroids of the muscle attachment areas on the bones; these points were treated as fixed

via points in the model. Since the medial and lateral heads are uniarticular, a single-cylinder obstacle set was used to model the way each of these muscles wraps around the distal humerus (Figure 4, paths 1 and 3). The long head of the triceps is biarticular, and so its path was modeled using a double-cylinder obstacle set: one cylinder was used to model the way in which the muscle winds over the neighboring

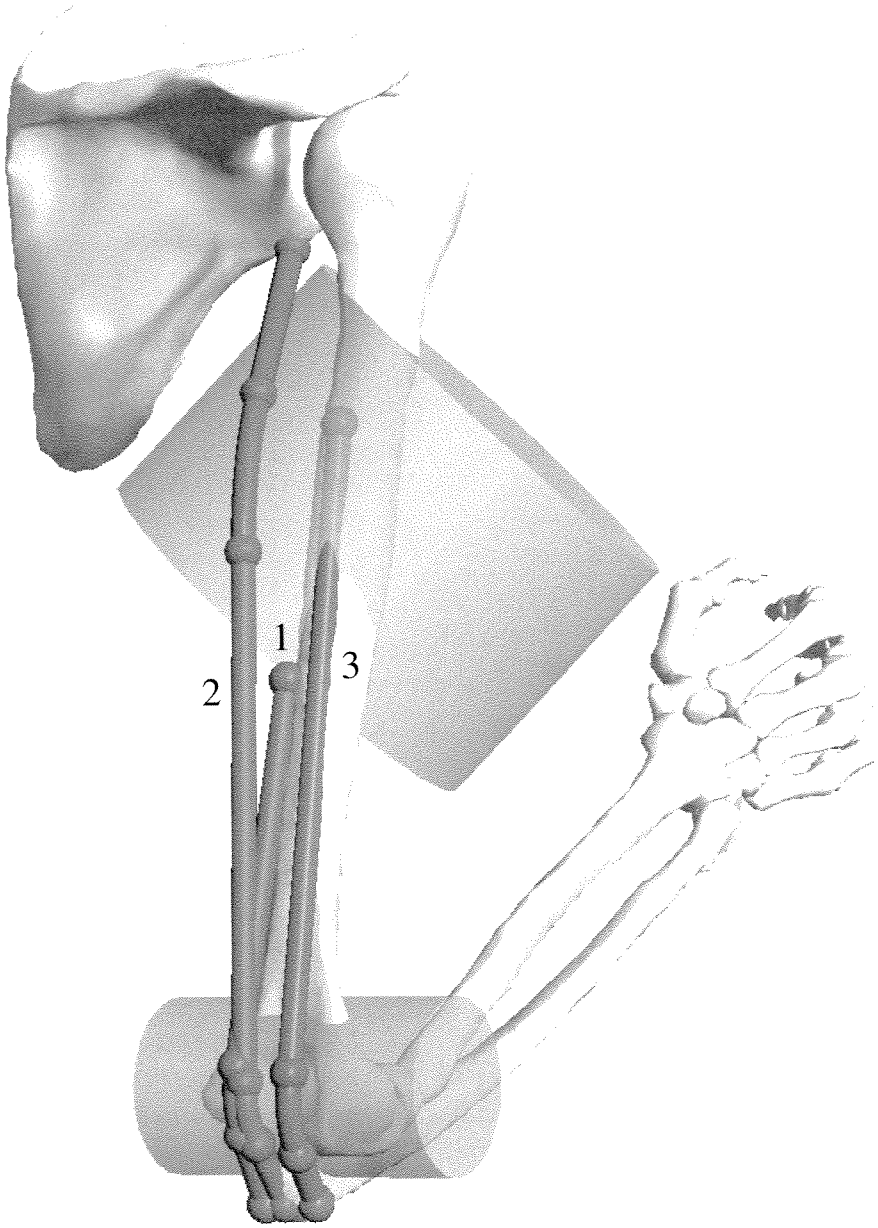

FIGURE 4 Posterolateral view of the obstacle-set model used to represent the paths of the three heads of triceps brachii. The medial head (1) and lateral head (3) are each modeled using a single-cylinder obstacle set (obstacles not shown). The long head (2) is modeled using a double-cylinder obstacle set as shown. The locations of the attachment sites of the muscle and the locations and orientations of the obstacles were chosen to reproduce the centroid paths of each head. The geometry of the bones and centroid paths of the muscles were obtained from three-dimensional reconstructions of the anatomical structures (see text).

muscles at the shoulder, while a second cylinder was used to model wrapping of the muscle around the condyles of the humerus (Figure 4, path 2).

Figure 5 shows the variation in the calculated and measured values of the moment arms as a function of elbow flexion angle. For the model, these moment arms were computed with the shoulder in the neutral position and the humerus lying alongside the torso. Good agreement between model and experiment over the full range of elbow flexion indicates that the paths of these muscles are represented accurately in the model (cf. gray and black lines). Consistent with the experimental data, the calculations show that all three heads of the triceps extend the elbow over the full range of joint movement [24,36,40]. As the elbow flexes from full extension to 56°, no contact occurs between the muscles and the bones, and the path of each muscle is represented by a straight line between origin and insertion. At flexion angles greater than 56°, the muscles wrap around the condyles of the humerus, and so the obstacle via points in the model become active. By accounting for the contact between the muscles and the bones, the computed extensor moment arms remain larger than if the muscle paths had been modeled simply by straight lines (Figure 5, black lines; see also Figure 9A below).

Deltoid

The deltoid is a large, thick triangular muscle which is composed of three parts: the anterior head, the middle head, and the posterior head. The anterior head originates from the outer third of the anterior border and upper surface of the clavicle; the middle

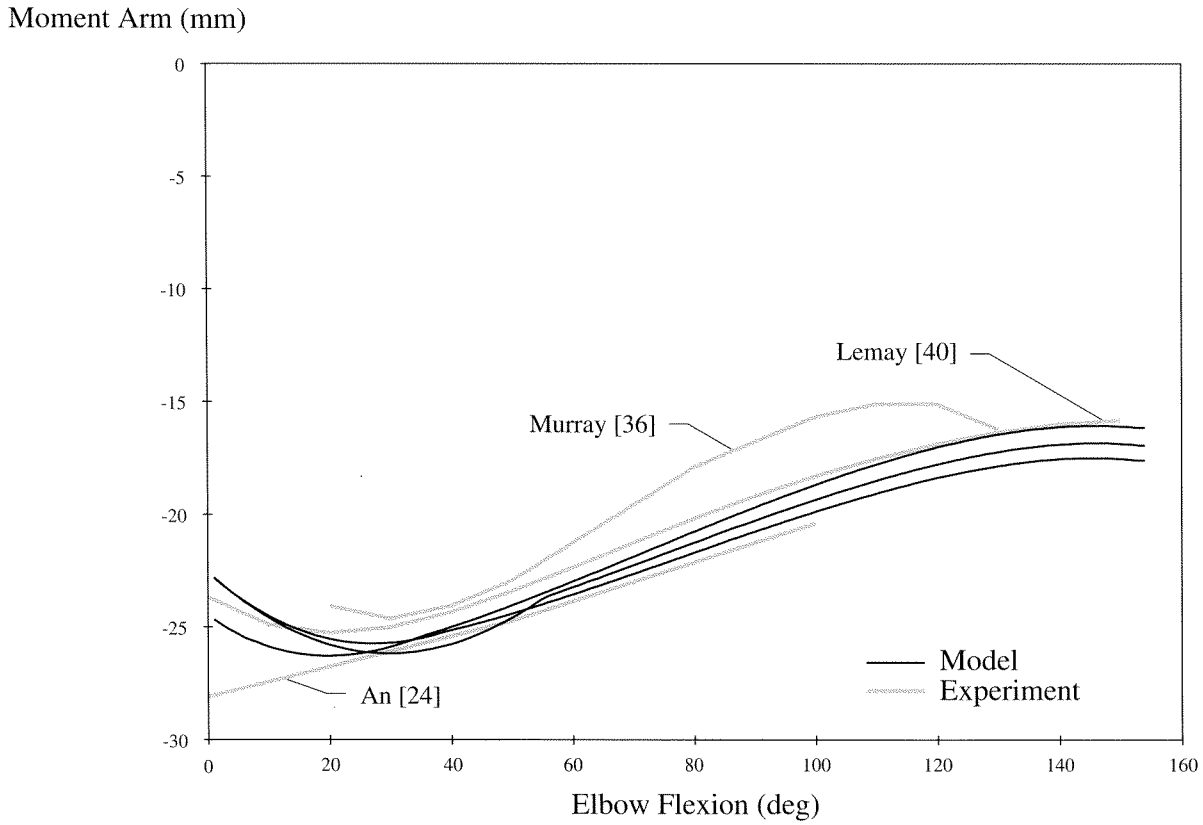

FIGURE 5 Comparison of measured moment arms (gray lines) and calculated moment arms (black lines) for the three heads of triceps brachii. The measurements were obtained from cadaver specimens; the calculated values were obtained using the obstacle-set model shown in Figure 4. Negative values of moment arm indicate elbow extension.

head originates from the outer margin and upper surface of the acromion process; and the posterior head originates from the lower lip of the posterior border of the spine of the scapula. All three heads cross the glenohumeral joint and unite to form a thick tendon, which inserts on the middle of the outer side of the shaft of the humerus.

Each head of the deltoid was represented by a separate and distinct muscle path with its own obstacle set. The origin and insertion of each path were found by inspecting transverse cross-sections of the muscle obtained from the VHM dataset and by calculating the centroids of the muscle attachment areas on the bones; these points were treated as fixed via points in the model. A sphere-capped cylinder was used to model the path of each muscle segment, since all three heads of deltoid are relatively long and the joint range of motion at the shoulder is relatively large (Figure 6, segments 1, 2, and 3). Although the dimensions of the sphere-capped cylinders are similar, the position and orientation of each obstacle is different, reflecting the fact that each head of the deltoid takes a substantially different course as it crosses over the shoulder.

Figure 7 shows the variation in the calculated and measured values of the moment arms of the deltoid as a function of shoulder abduction. In the model and in the experiments [35], the shaft of the humerus was constrained to move in the plane of the scapula, with no combined axial rotation. Consistent with experiment, the calculated moment arms vary almost linearly with abduction. The middle and posterior heads, respectively, cause abduction and adduction of the shoulder over the entire range of joint movement in the scapular plane; the anterior head causes either adduction or abduction, depending upon the relative orientation of the bones in the scapular plane (cf. Anterior, Middle, and Posterior in Figure 7).

Effect of Muscle-Path Modeling

To illustrate the differences between the straight-line model, the fixed-via-point model, and the obstacle-set model, each was used to calculate the length and moment arm of the long head of the triceps brachii as a function of elbow flexion. For these calculations, the upper arm was positioned alongside the torso with the humerus either in neutral rotation or in 45° internal rotation. In each model, the locations of the origin and insertion sites were identical. The obstacle-set model has been described previously (see Triceps and Figure 4 above). The path of the muscle in the fixed-via-point model was designed to closely follow the path prescribed in the obstacle-set model with the shoulder in the neutral position. Specifically, the via points in the fixed-via-point model were chosen to lie on the surface of the cylinder in the obstacle-set model. Furthermore, the elbow flexion angles at which these via points become active or inactive were selected so that the muscle length changed smoothly as the elbow flexion angle was varied with the shoulder in the neutral position.

The lengths and moment arms obtained by the straight-line model are noticeably different from those obtained by the fixed-via-point and obstacle-set models at large flexion angles of the elbow (Figures 8 and 9). The straight-line model also yields values of the moment arm which are significantly different from measurements reported in the literature (cf. Straight in Figure 9A with gray lines in Figure 5). Perhaps most significantly, at flexion angles greater than 120°, the straight-line model indicates that the long head of the triceps acts to flex the elbow, whereas the fixed-via-point and obstacle-set models both show, in agreement with experiment, that the muscle acts to extend the elbow throughout the range of joint movement (cf. Straight with Fixed and Obstacle in Figure 9A).

With the shoulder in the neutral position, all three models yield identical values for the muscle lengths and moment arms between 0 and 56° of elbow flexion. At these angles, the path of the muscle in each model is defined by a straight line between the origin and insertion (Figures 8 and 9, solid lines). At flexion angles greater than 56°, additional via points become active in the obstacle-set and fixed-via-point models in order to account for contact between the muscle and the humeral condyles. Although the

FIGURE 6 Posterolateral view of the obstacle-set model used to represent the paths of the three heads of deltoid. The anterior head (1), middle head (2), and posterior head (3) are each modeled using a sphere-capped cylinder obstacle set. Only the obstacle-set used to model the middle head (2) is shown. The paths of the three heads are modeled using different sizes, positions, and orientations for the obstacles. The locations of the attachment sites of the muscle and the locations and orientations of the obstacles were chosen to reproduce the centroid paths of each head. The geometry of the bones and centroid paths of the muscles were obtained from three-dimensional reconstructions of the anatomical structures.

muscle lengths and moment arms calculated by these two models are in close agreement at large flexion angles, minor differences are apparent.

With the shoulder in the neutral position and the elbow flexed beyond 56°, the moment arm curves for the fixed-via-point model are characterized by a series of concave-upward line segments joined together by corners (Figure 9A, Fixed). Each corner is the result of a fixed via point becoming active at a particular elbow flexion angle. If a fixed via

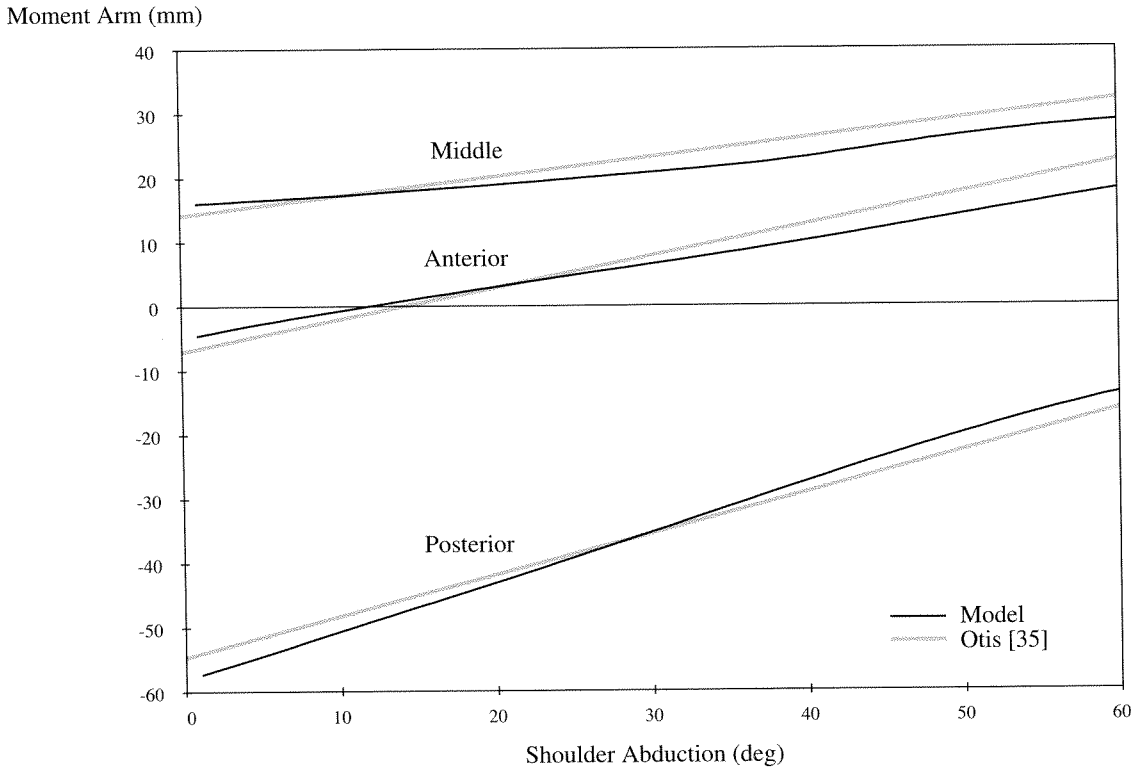

FIGURE 7 Comparison of measured moment arms (gray lines) and calculated moment arms (black lines) for the three heads of deltoid. The measurements were obtained from cadaver specimens; the calculated values were obtained using the obstacle-set model shown in Figure 6. Positive values of moment arm indicate shoulder abduction.

point was not added to the muscle path at each of these flexion angles, the moment arm curves would continue their concave-upward trend, thereby mimicking the results obtained by the straight-line model (Figure 9A, Straight). By adding a new via point, a new straight-line model is initiated that more closely approximates the path of the real muscle in the region of flexion where the via point became active. In contrast, the moment arm curves obtained by the obstacle-set model exhibit only one corner at 56°, which corresponds to the flexion angle at which the obstacle via points become active (Figure 9A, Obstacle). Beyond 56° of elbow flexion, the obstacle-set moment arm curves are smooth and bend concave-downwards, much like the curves obtained from experiment (cf. Obstacle in Figure 9A with gray lines in Figure 5). This result is indicative of the fact that the obstacle-set model accounts for the actual, curved path of the muscle.

Between 0 and 56° of elbow flexion, the lengths and moment arms obtained by each model are slightly different for the neutral and internally-rotated positions of the shoulder (cf. solid and dotted lines in Figure 9A). This occurs because a change in the configuration of the shoulder causes the attachment sites of the muscle to move relative to each other. For the straight-line and obstacle-set models, the difference in muscle moment arms between the two shoulder positions continues throughout the range of elbow flexion because each of these models continues to take into account the change in the relative positions of the muscle attachment sites. In the fixed-via-point model, however, the moment arms are exactly the same at all flexion angles greater than 56°, irrespective of the shoulder position (compare solid and dotted lines for Fixed in Figure 9A). Once the first fixed via point becomes active for a given shoulder position, the length of the path segment

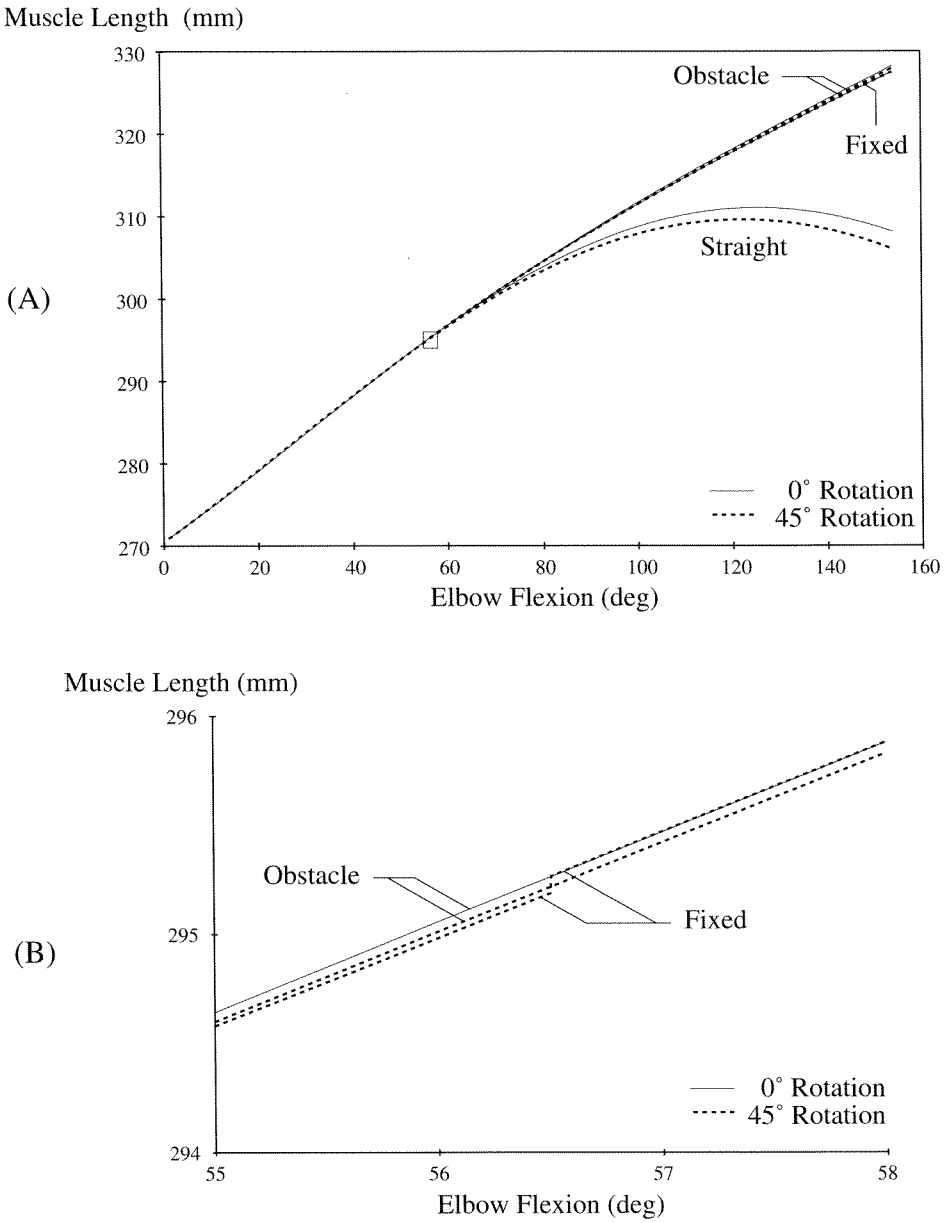

FIGURE 8 (A) Comparison of muscle lengths for the long head of triceps obtained using the straight-line model (Straight), fixed-via-point model (Fixed), and obstacle-set model (Obstacle). For each model, muscle length was computed over the entire range of elbow flexion with the humerus positioned alongside the torso in neutral rotation (solid lines) and in 45° internal rotation (dotted lines). (B) Expanded scale of the graph in (A), where the muscle lengths obtained using the fixed-via-point and obstacle-set models are shown near the elbow flexion angle where the muscle first begins to wrap around the obstacle (cylinder) at the elbow. The fixed-via-point model produces a discontinuity in muscle length when the shoulder is rotated 45° internally (Fixed, dotted line).

between the origin and the fixed via point is fixed, and subsequent changes in muscle length depend only on the flexion angle of the elbow. Consequently, at the flexion angle where the first via point becomes active, a discontinuity results in the muscle length, and therefore in the moment arm, for shoulder positions other than neutral (dotted lines for Fixed in Figures 9A and B). Because the locations

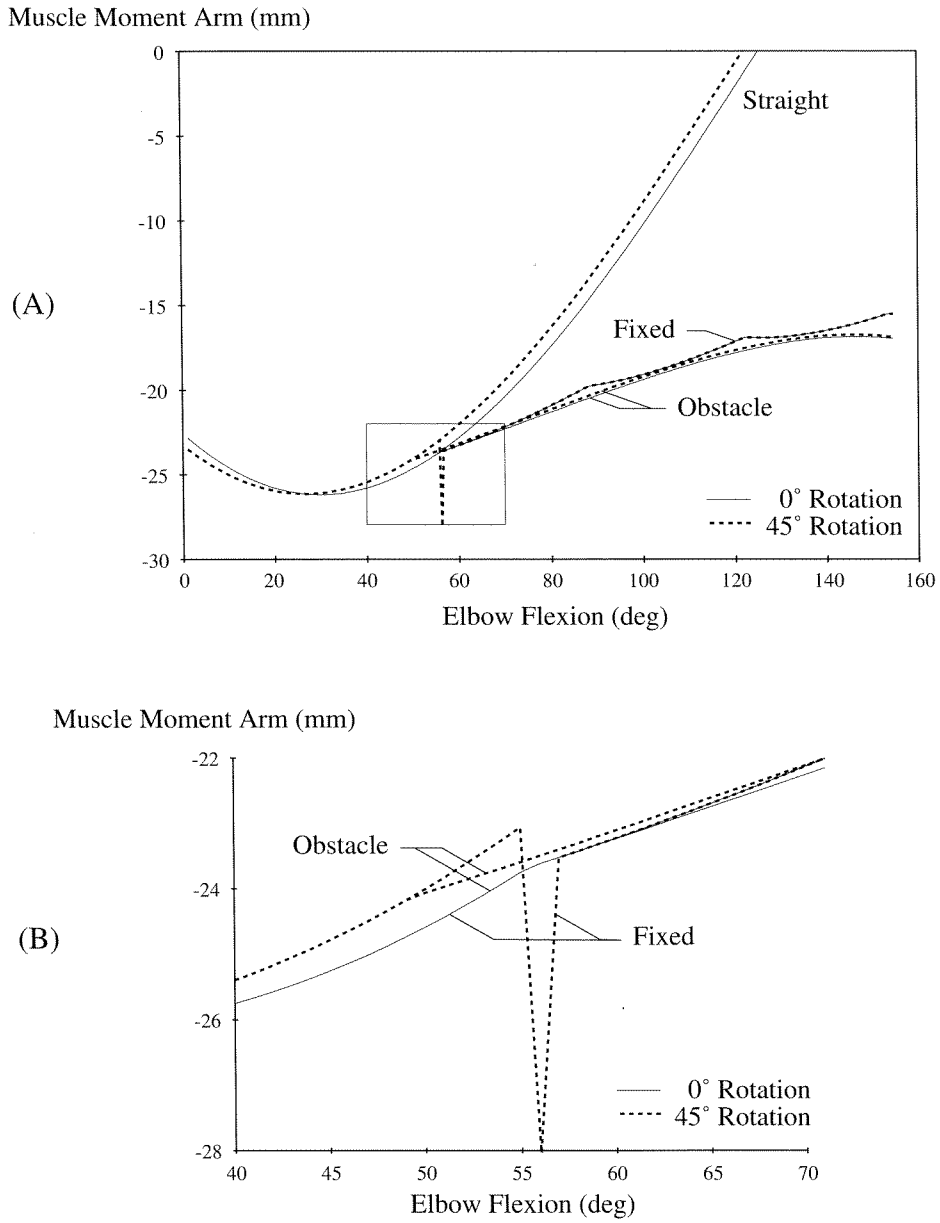

FIGURE 9 (A) Comparison of moment arms for the long head of triceps obtained using the straight-line model (Straight), fixed-via-point model (Fixed), and obstacle-set model (Obstacle). For each model, the moment arms were computed over the entire range of elbow flexion with the humerus positioned alongside the torso in neutral rotation (solid lines) and in 45° internal rotation (dotted lines). (B) Expanded scale of the graph in (A), where the moment arms obtained using the fixed-via-point and obstacle-set models are shown near the elbow flexion angle where the muscle first begins to wrap around the obstacle (cylinder) at the elbow. The fixed via-point model produces a discontinuity in moment arm when the shoulder is rotated 45° internally (Fixed, dotted line).

of the via points for the fixed-via-point model were chosen with the shoulder in neutral rotation, those via-point locations are valid only for that particular configuration of the joint. This result illustrates a major limitation of the fixed-via-point model when it is used to represent the paths of muscles at joints which have more than one rotational degree of freedom.

DISCUSSION

The obstacle-set model approximates the centroid path of a muscle for all configurations of the joint. It therefore shares many of the same limitations with other centroid-line models such as the fixed-via-point model. First, determining the actual centroid path of a muscle is difficult and requires a large database, particularly if the joint configuration changes. Centroid paths can usually be obtained only for a limited number of muscles and only for a single configuration of the joint. Second, centroid paths derived from cadaver measurements will generally underestimate the distance between the muscle centroid line-of-action and the joint axis of rotation because muscle tone is neglected in these measurements. In this respect, the straight-line model may produce a better approximation of the true muscle path than its centroid-line counterpart [19]. Third, assuming that the muscle force acts along the centroids of the muscle cross-sections presumes that the attachment sites can be modeled as single points. This assumption may be reasonable for muscles which attach over relatively small areas of the bones (e.g., medial and lateral heads of gastrocnemius on the distal femur), but it is undoubtedly limiting for broad, fan-shaped muscles which attach over larger regions (e.g., serratus anterior, subscapularis, and infraspinatus on the scapula). One way to circumvent this difficulty is to model the muscle using several distinct paths. For example, Hogfors *et al.* [32] modeled the action of the trapezius by dividing the muscle into four separate paths, with the origin and insertion of each path represented as single points. In a later study, Van der Helm and Veenbaas [41] showed that no more than six paths are needed to accurately model the action of any muscle in the body.

Despite the above limitations, the obstacle-set model for representing muscle paths is more accurate than previous models reported in the literature [19,20,27]. While the straight-line model may produce reasonable results under certain circumstances [19,42], it cannot provide meaningful results over an entire range of motion for many of the joints. In the case of the long head of the triceps brachii, for example, contrary to experimental findings, the straight-line model causes the triceps to *flex* rather than extend the elbow at large flexion angles of the joint (cf. Straight in Figure 9A with gray lines in Figure 5). Although the fixed-via-point model accounts for the effects of neighboring anatomical constraints, it does not allow for the possibility of relative movement between the muscle and the constraints. As indicated by the results of Figures 8 and 9, discontinuities in the calculated length and moment arm of the muscle may occur as a result of this limitation. The obstacle-set model accounts not only for the interaction between the muscle path and the neighboring anatomical constraints, but also for how this interaction changes with a change in joint configuration. Consequently, the obstacle-set model is the only model that can be used to represent the paths of muscles which cross joints with multiple degrees of freedom (e.g., deltoid at the shoulder).

Although the obstacle-set model can provide an accurate representation of a muscle's path, the positions of all fixed via points and the positions and orientations of all obstacles must be carefully chosen in order to reproduce the actual path of the muscle for the entire range of joint movement. There are two necessary and sufficient conditions for ensuring that this requirement is met: first, the model must accurately reproduce the centroid path of the muscle for an arbitrary joint configuration; and second, the model must accurately reproduce the moment arms of the muscle over the full range of joint movement. Since the moment arm of the muscle is equal to the total derivative of muscle length with respect to joint angle, these two conditions should guarantee that the actual muscle path is represented accurately in the model for all configurations of the joint. (See Pandy [43] for a review of muscle moment arms.)

In order to model the muscle centroid path for an arbitrary joint configuration, the actual muscle centroid path must be known for the configuration in question. The actual centroid path can be found by reconstructing two-dimensional medical images obtained either from cadaver specimens or from living people. Using the reconstructed muscle

centroid path as a reference, the locations of the fixed via points and the positions and orientations of the obstacles can be chosen so that the muscle path is accurately modeled for the given joint configuration. In this study, the obstacle-set models of the triceps brachii and deltoid muscles were developed using a computer graphics workstation and a Graphical User Interface, which enabled the obstacle-set parameters to be interactively adjusted so as to reproduce the muscle centroid paths obtained from the reconstructed bones and muscles of the VHM male cadaver.

Once the muscle centroid path has been modeled for one configuration of the joint, the moment arms calculated in the model can be compared with measured values obtained over the entire range of joint movement (Figure 5, gray and black lines). If needed, minor trial-and-error adjustments can then be made to the locations of the fixed via points and/or to the locations and orientations of the obstacles until an acceptable level of agreement is found between model and experiment. Once again, in this study a computer graphics workstation and a Graphical User Interface were used to make such adjustments and to visualize the effects of these changes on the paths of the modeled muscles.

APPENDIX A — WRAPPING CONDITION

Step 3 of the obstacle-set algorithm is to determine whether or not, for a given joint configuration, a muscle path wraps around an obstacle; that is, whether or not the obstacle via points are active (see Figure 3, Step 3). This *wrapping condition* changes with joint configuration because the bounding-fixed via points move with respect to the obstacle. Mathematically, the wrapping condition is defined in terms of the angle formed by the muscle path as it wraps over the surface of an obstacle (see Figure A). If the *wrapping angle* is greater than 180°, we conclude that wrapping should *not* occur.

A computationally efficient way to determine whether the wrapping angle exceeds 180° is to examine the orientation of the two obstacle via points relative to the center of the obstacle in the plane normal to the curvature of wrapping. Appendices C–F describe how the coordinates of the obstacle via points are computed for each obstacle in this plane. In general, the relative orientation of three points in a plane can be determined by calculating the determinant of the following matrix:

$$\text{Det} = \begin{vmatrix} X_1 & Y_1 & 1 \\ X_2 & Y_2 & 1 \\ X_3 & Y_3 & 1 \end{vmatrix}$$

$$\Rightarrow \begin{cases} \text{if Det} > 0 \text{ orientation is} \\ \quad \text{counter clockwise} \\ \text{if Det} = 0 \text{ points are colinear} \\ \text{if Det} < 0 \text{ orientation is clockwise} \end{cases} \tag{A.1}$$

where (X_1, Y_1), (X_2, Y_2), and (X_3, Y_3) are the xy coordinates of the three points in question. For our case, if the origin of an xy coordinate system is centered at the obstacle center in the plane of curvature, then the wrapping condition reduces to:

$$\text{Det} = (Q_x T_y - Q_y T_x) \Rightarrow \text{if}(R)(\text{Det}) < 0, \quad \text{then wrapping does } \textit{not} \text{ occur} \tag{A.2}$$

where (Q_x, Q_y) are the coordinates of the first obstacle via point, (T_x, T_y) are the coordinates of the second obstacle via point, (0,0) is the origin of the coordinate system, and R is the obstacle radius (the sign of the radius determines the wrapping direction — see Appendix B).

APPENDIX B — CIRCLE TANGENCY

Step 2 of the obstacle-set algorithm is to compute the locations of the obstacle via points associated with an obstacle (see Figure 3, Step 2). By definition, obstacle via points are located on the surface of an obstacle. To ensure a minimum-distance muscle path, straight-line segments which join the obstacle via points to their neighboring bounding-fixed via points must be tangent to the obstacle surface. These two geometric conditions, together with the fact that both a sphere and a cylinder are circular in cross-section, may be used to calculate the coordinates of the obstacle via points

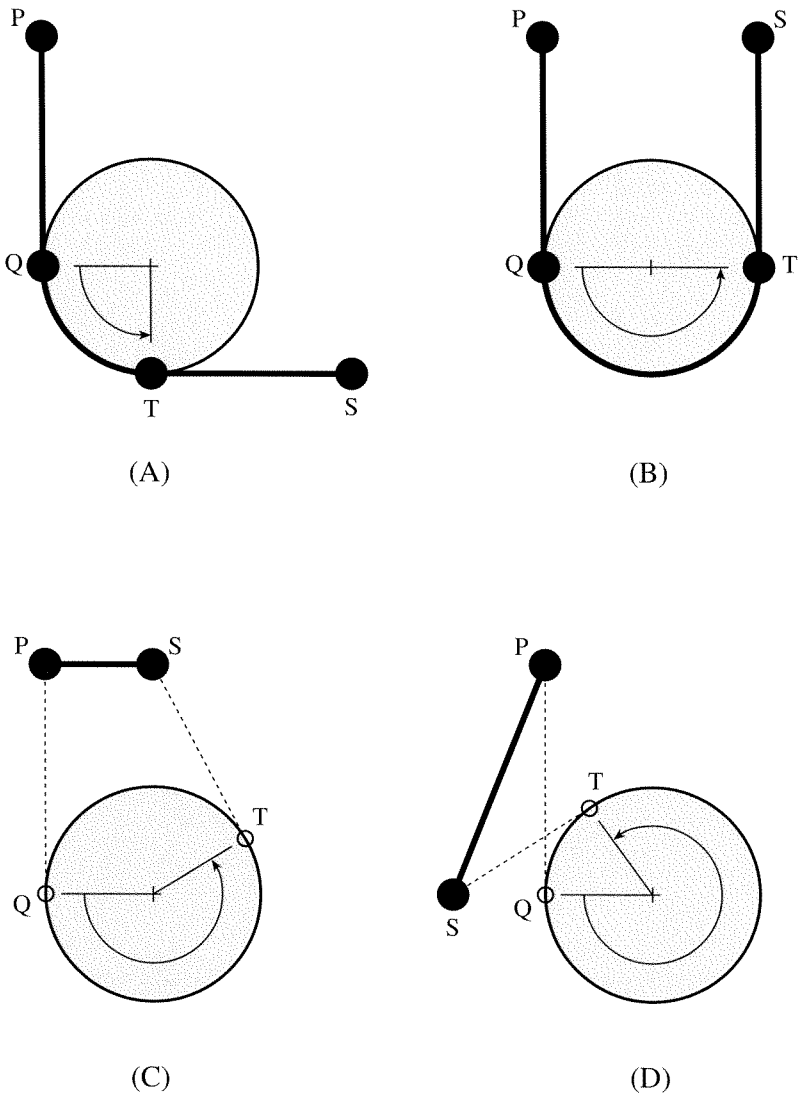

FIGURE A Illustration of the wrapping condition. In each configuration, the obstacle set consists of two bounding-fixed via points, $\boldsymbol{P}$ and $\boldsymbol{S}$, two obstacle via points, $\boldsymbol{Q}$ and $\boldsymbol{T}$, a single obstacle, and the muscle path between $\boldsymbol{P}$ and $\boldsymbol{S}$. The locations of $\boldsymbol{Q}$ and $\boldsymbol{T}$ are computed using the tangency equations for right-handed wrapping described in Appendix B. The wrapping condition is based on the angle formed by the arc from $\boldsymbol{Q}$ to $\boldsymbol{T}$, referred to as the *wrapping angle* (see text). In (A) the wrapping angle is less than 180° and in (B) the wrapping angle is equal to 180°. Thus, in these configurations, the obstacle via points are assumed to be active, and the muscle path passes through them. In (C) and (D), because the wrapping angle is greater than 180°, the obstacle via points are assumed to be inactive, and the muscle path does not pass through these points.

in the plane of the cross-section (i.e. two of the three coordinates for each obstacle via point may be found). Appendices C–F describe how to define the plane of cross-section for each obstacle within an obstacle set.

Consider a generic obstacle set with two bounding-fixed via points, $\boldsymbol{P}$ and $\boldsymbol{S}$, two obstacle via points, $\boldsymbol{Q}$ and $\boldsymbol{T}$, and one obstacle with radius R and center point $\boldsymbol{O}$ (see Figure B). In the plane of the cross-section, the obstacle is described by a circle. The problem is to compute the locations of $\boldsymbol{Q}$ and $\boldsymbol{T}$ given the locations of $\boldsymbol{P}$ and $\boldsymbol{S}$, subject to the geometric conditions noted above. Focusing on line segment $\boldsymbol{PQ}$, two constraint equations may be derived:

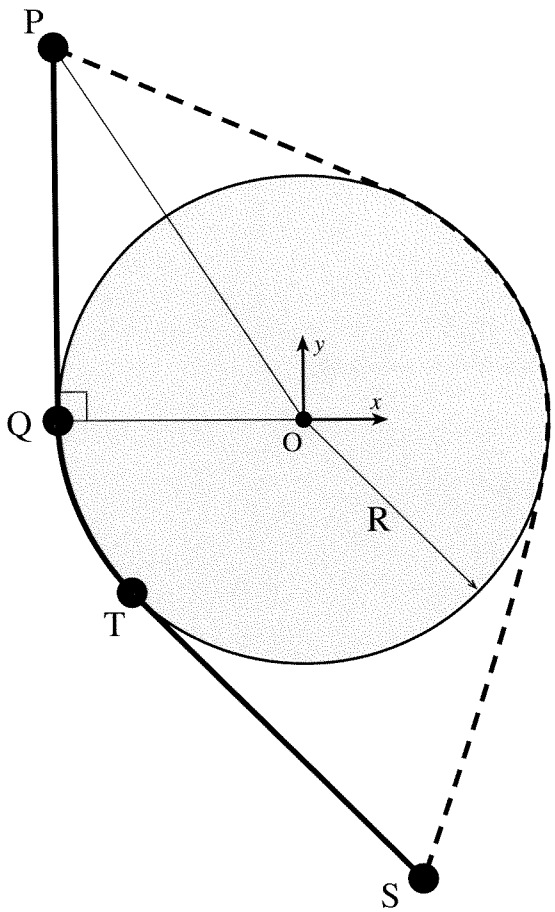

FIGURE B Illustration of the circle tangency and wrapping direction. The obstacle set consists of two bounding fixed via points, ***P*** and ***S***, two obstacle via points, ***Q*** and ***T***, a single obstacle of radius R, and the muscle path between ***P*** and ***S***. The xy coordinates of ***Q*** and ***T*** are computed using the tangency constraint equations and the known locations of ***P*** and ***S***. Two sets of solutions are possible: one solution leads the path to wrap around the obstacle in a *right-handed* sense (thick solid line); the other solution leads the path to wrap in a *left-handed* sense (thin dotted line).

$$R^2 = Q_x^2 + Q_y^2 \tag{B.1}$$

$$R^2 + (P_x - Q_x)^2 + (P_y - Q_y)^2 = P_x^2 + P_y^2 \tag{B.2}$$

These equations may be combined, squared, and rearranged to eliminate Q_y:

$$R^4 = P_x^2 Q_x^2 + P_y^2(R^2 - Q_x^2) + 2P_x Q_x(R^2 - P_x Q_x) \tag{B.3}$$

Using the quadratic formula, the solution for Q_x is:

$$Q_x = \frac{P_x R^2 \pm R P_y \sqrt{P_x^2 + P_y^2 - R^2}}{(P_x^2 + P_y^2)} \tag{B.4}$$

Similarly, the solution for Q_y is:

$$Q_y = \frac{P_y R^2 \mp R P_x \sqrt{P_x^2 + P_y^2 - R^2}}{(P_x^2 + P_y^2)} \tag{B.5}$$

Equations B.4 and B.5 each have two solutions, corresponding to the two possible directions which the path can take around the circle. If the top solution set is used ("+" in B.4 and "−" in B.5) the path will wrap in a right-handed sense (with respect to the z-axis) from ***P*** to ***S***. If the bottom solution set is used ("−" in B.4 and "+" in B.5) the path will wrap in a left-handed sense. Either wrapping direction can be specified by always using the top

solution set and giving a signed value to the radius, R. In this way, positive and negative values for R would correspond to right-handed and left-handed wrapping, respectively. The top solution set for $\boldsymbol{Q}$, and the analogous solution set for $\boldsymbol{T}$ (note the sign reversal) are:

$$Q_x = \frac{P_x R^2 + R P_y \sqrt{P_x^2 + P_y^2 - R^2}}{(P_x^2 + P_y^2)}$$

$$Q_y = \frac{P_y R^2 - R P_x \sqrt{P_x^2 + P_y^2 - R^2}}{(P_x^2 + P_y^2)} \quad \text{(B.6)}$$

$$T_x = \frac{S_x R^2 - R S_y \sqrt{S_x^2 + S_y^2 - R^2}}{(S_x^2 + S_y^2)}$$

$$T_y = \frac{S_y R^2 + R S_x \sqrt{S_x^2 + S_y^2 - R^2}}{(S_x^2 + S_y^2)} \quad \text{(B.7)}$$

Step 4 of the obstacle-set algorithm is to compute the segment lengths of the respective muscle path segments (see Figure 3, Step 4). It is convenient, while doing calculations in the plane of the cross-section of the obstacle, to also compute the planar component of the segment lengths (see Appendices C–F). The planar components of the straight-line segments, $\|\boldsymbol{PQ}\|_{xy}$ and $\|\boldsymbol{TQ}\|_{xy}$, may be computed simply as the straight-line distance between the respective points. The planar component of the arc length of segment $\|\boldsymbol{QT}\|_{xy}$ is found using the law of cosines, thus:

$$\|\boldsymbol{QT}\|_{xy} = \left| R \cos^{-1}\left(1 - \frac{(T_x - Q_x)^2 + (T_y - Q_y)^2}{2R^2}\right)\right| \quad \text{(B.8)}$$

APPENDIX C — SINGLE SPHERE OBSTACLE-SET ALGORITHM

This version of the obstacle-set algorithm computes the minimum-distance path around a single-sphere obstacle set (see Figures C and 2A). The locations of the sphere center, $\boldsymbol{O}$, and the bounding-fixed via points, $\boldsymbol{P}$ and $\boldsymbol{S}$, are known and are assumed to be expressed in the sphere reference frame (Figure C, Step 1). The locations of the obstacle via points, $\boldsymbol{Q}$ and $\boldsymbol{T}$, are computed based on the fact that all points along the minimum-distance path around a sphere lie in a plane which passes through the center of the sphere.

Reference Frame

$\boldsymbol{O}$ ⇒ origin of frame, center of the sphere

Axes ⇒ orthonormal, arbitrarily oriented

Parameters

R ⇒ radius of sphere (positive only — see Appendix B)

Inputs

$\boldsymbol{P}$ ⇒ bounding-fixed via point, start of path

$\boldsymbol{S}$ ⇒ bounding-fixed via point, end of path

Outputs

$\boldsymbol{Q}$ ⇒ obstacle via point, start of path which contacts the sphere

$\boldsymbol{T}$ ⇒ obstacle via point, end of path which contacts the sphere

Lengths ⇒ lengths of path segments between $\boldsymbol{P}$, $\boldsymbol{Q}$, $\boldsymbol{T}$, and $\boldsymbol{S}$

Compute Locations of Obstacle Via Points (Figure C, Step 2)

Based on the condition mentioned above, points $\boldsymbol{O}$, $\boldsymbol{P}$, $\boldsymbol{Q}$, $\boldsymbol{T}$, and $\boldsymbol{S}$, lie in a common plane. This plane may be defined from the known locations of $\boldsymbol{O}$, $\boldsymbol{P}$, and $\boldsymbol{S}$. We define the plane in terms of a temporary reference frame whose z-axis is normal to the plane and whose origin is at the center of the sphere. The rotation matrix transforming point coordinates from the sphere reference frame to the plane reference frame may be computed as:

$$\boldsymbol{M} = \begin{bmatrix} \overline{\boldsymbol{OS}} \\ \hat{\boldsymbol{N}} \times \overline{\boldsymbol{OS}} \\ \hat{\boldsymbol{N}} \end{bmatrix} \Rightarrow 3 \times 3 \text{ rotation matrix} \quad \text{(C.1)}$$

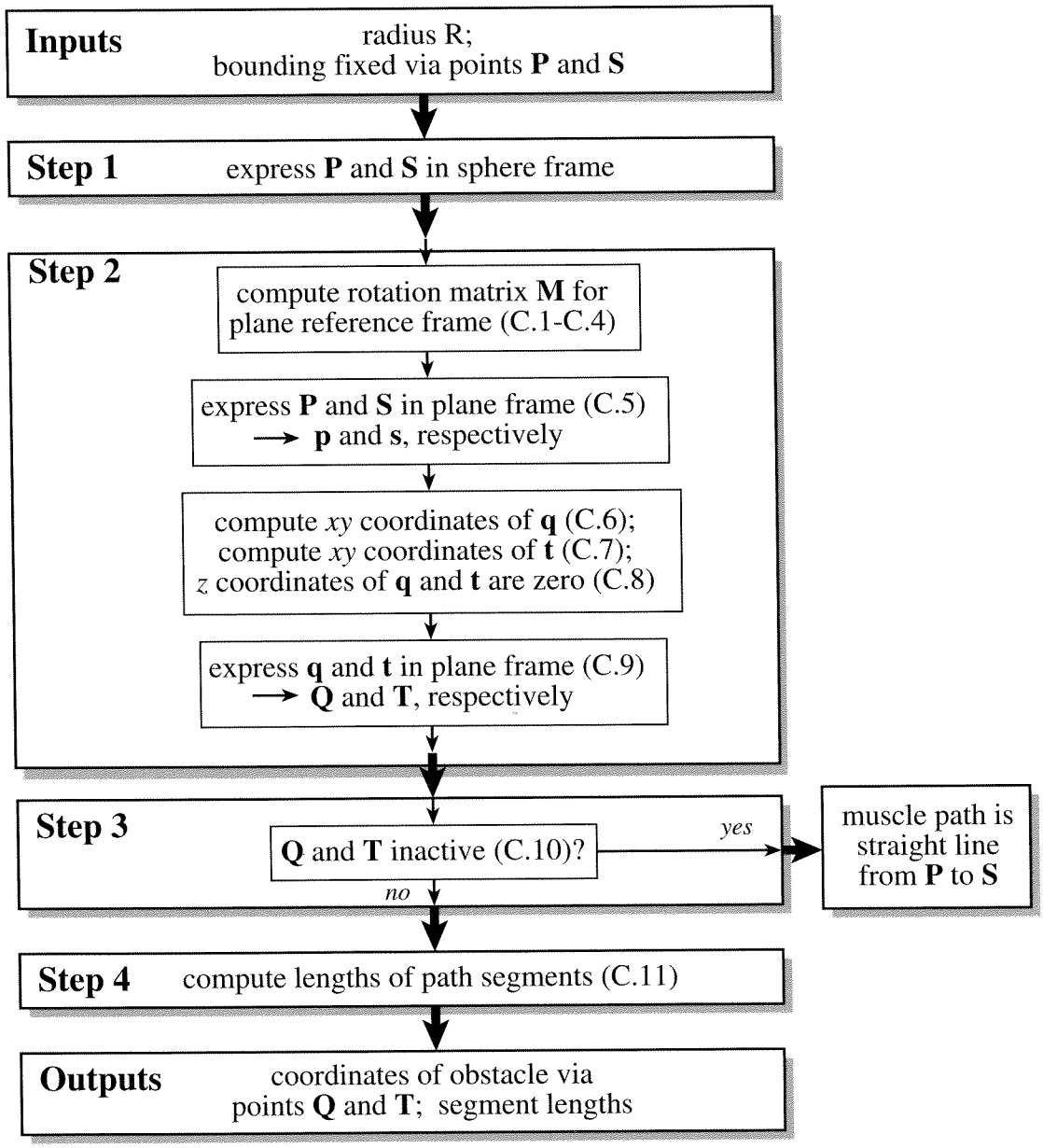

FIGURE C Flowchart of the single-sphere obstacle-set algorithm. Symbols are defined in the text.

where

$$\overline{OS} = \frac{[S_x, S_y, S_z]}{\sqrt{S_x^2 + S_y^2 + S_z^2}}$$

$\Rightarrow$ the unit vector from O to S (C.2)

$\hat{N} = \overline{OP} \times \overline{OS} \Rightarrow$ the unit vector normal to the plane (z-axis) (C.3)

$$\overline{OP} = \frac{[P_x, P_y, P_z]}{\sqrt{P_x^2 + P_y^2 + P_z^2}} \Rightarrow \text{the unit vector from } O \text{ to } P \quad \text{(C.4)}$$

Points P and S may then be expressed in the plane reference frame by a simple transformation (points expressed in the plane reference frame will

be written in lower case):

$$\boldsymbol{p} = [\boldsymbol{M}]\boldsymbol{P} \qquad \boldsymbol{s} = [\boldsymbol{M}]\boldsymbol{S} \tag{C.5}$$

Within the plane reference frame, the locations of points $\boldsymbol{q}$ and $\boldsymbol{t}$ may be found using the circle tangency equations (see Appendix B):

$$q_x = \frac{p_x R^2 + R p_y \sqrt{p_x^2 + p_y^2 - R^2}}{(p_x^2 + p_y^2)}$$

$$q_y = \frac{p_y R^2 - R p_x \sqrt{p_x^2 + p_y^2 - R^2}}{(p_x^2 + p_y^2)} \tag{C.6}$$

$$t_x = \frac{s_x R^2 - R s_y \sqrt{s_x^2 + s_y^2 - R^2}}{(s_x^2 + s_y^2)}$$

$$t_y = \frac{s_y R^2 + R s_x \sqrt{s_x^2 + s_y^2 - R^2}}{(s_x^2 + s_y^2)} \tag{C.7}$$

$$q_z = 0 \qquad t_z = 0 \tag{C.8}$$

These points are then expressed in the sphere reference frame, thus:

$$\boldsymbol{Q} = [\boldsymbol{M}]^T \boldsymbol{q} \qquad \boldsymbol{T} = [\boldsymbol{M}]^T \boldsymbol{t} \tag{C.9}$$

Determine Wrapping Conditions (Figure 3, Step 3)

To determine whether or not $\boldsymbol{Q}$ and $\boldsymbol{T}$ are active, the wrapping conditions (see Appendix A) may be applied using $\boldsymbol{Q}$ and $\boldsymbol{T}$ expressed in the plane reference frame (i.e; Equation A.2 is used with $\boldsymbol{q}$ and $\boldsymbol{t}$ defined as in Equations C.6 to C.8)

$$\text{Det} = (q_x t_y - q_y t_x) \Rightarrow \text{if } (R)(\text{Det}) < 0, \text{ then wrapping does } \textit{not} \text{ occur} \tag{C.10}$$

Compute Muscle Segment Lengths (Figure 3, Step 4)

If points $\boldsymbol{Q}$ and $\boldsymbol{T}$ are inactive, the minimum-distance path is simply a straight line between points $\boldsymbol{P}$ and $\boldsymbol{S}$. Otherwise, the minimum-distance path traverses from $\boldsymbol{P}$, through $\boldsymbol{Q}$, around the sphere to $\boldsymbol{T}$, and terminates at $\boldsymbol{S}$ (see Figure 2A). The lengths of segments $\boldsymbol{PQ}$ and $\boldsymbol{TS}$ may be computed simply as the straight-line distance between the respective points. The arc length of line segment $\boldsymbol{QT}$ is found using the law of cosines, thus:

$$\|\boldsymbol{QT}\| = R\text{Cos}^{-1}\left(1.0 - \frac{(q_x - t_x)^2 + (q_y - t_y)^2}{2R^2}\right) \tag{C.11}$$

APPENDIX D — SINGLE CYLINDER OBSTACLE-SET ALGORITHM

This version of the obstacle-set algorithm computes the minimum-distance path around a single-cylinder obstacle set (see Figures D and 2B). The locations of the origin of the cylinder reference frame, $\boldsymbol{O}$, and the bounding-fixed via points, $\boldsymbol{P}$ and $\boldsymbol{S}$, are known and are assumed to be expressed in the cylinder reference frame (Figure D, Step 1). The locations of the obstacle via points are computed based on the fact that the minimum-distance path around a cylinder forms a straight line in the space tangent to and wrapping around the cylinder (like a straight line drawn on a piece of paper wrapped around the cylinder).

Reference Frame

$\boldsymbol{O}$ ⇒ origin of frame, any convenient point on the axis of the cylinder

Axes ⇒ z-axis aligned with axis of the cylinder, x- and y-axes orthonormal

Parameters

R ⇒ radius of cylinder (positive or negative — see Appendix B)

Inputs

$\boldsymbol{P}$ ⇒ bounding-fixed via point, start of path

$\boldsymbol{S}$ ⇒ bounding-fixed via point, end of path

Outputs

$\boldsymbol{Q}$ ⇒ obstacle via point, start of path contact with cylinder

$\boldsymbol{T}$ ⇒ obstacle via point, end of path contact with cylinder

Lengths ⇒ lengths of respective path segments between $\boldsymbol{P}$, $\boldsymbol{Q}$, $\boldsymbol{T}$, and $\boldsymbol{S}$

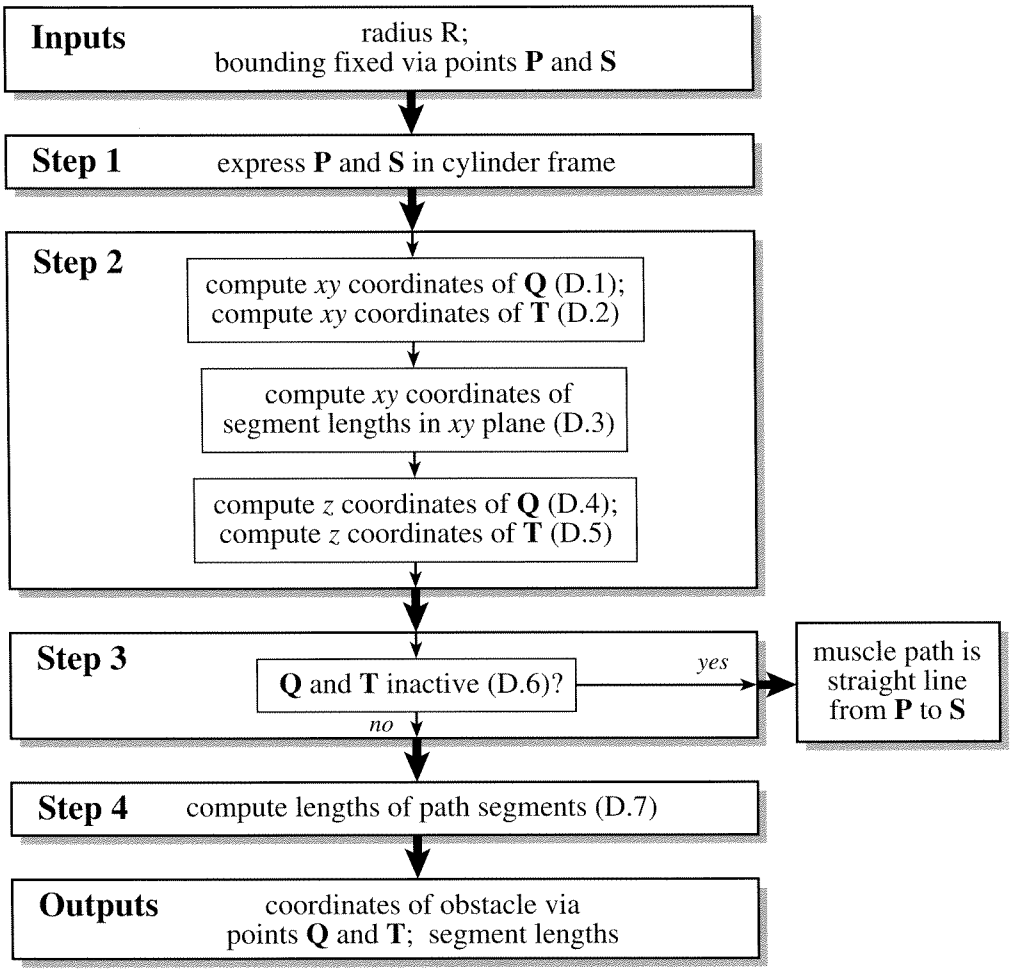

FIGURE D Flowchart of the single-cylinder obstacle-set algorithm. Symbols are defined in the text.

Compute Locations of Obstacle Via Points (Figure D, Step 2)

The projection of the cylinder onto the xy-plane of the cylinder reference frame is a circle. Because the line segments $\boldsymbol{PQ}$ and $\boldsymbol{TS}$ must be tangent to the cylinder, the x and y coordinates of $\boldsymbol{Q}$ and $\boldsymbol{T}$ may be found using the circle tangency equations (Appendix B), thus:

$$Q_x = \frac{P_x R^2 + R P_y \sqrt{P_x^2 + P_y^2 - R^2}}{(P_x^2 + P_y^2)}$$

$$Q_y = \frac{P_y R^2 - R P_x \sqrt{P_x^2 + P_y^2 - R^2}}{(P_x^2 + P_y^2)} \qquad \text{(D.1)}$$

$$T_x = \frac{S_x R^2 - R S_y \sqrt{S_x^2 + S_y^2 - R^2}}{(S_x^2 + S_y^2)}$$

$$T_y = \frac{S_y R^2 + R S_x \sqrt{S_x^2 + S_y^2 - R^2}}{(S_x^2 + S_y^2)} \qquad \text{(D.2)}$$

The z coordinates of $\boldsymbol{Q}$ and $\boldsymbol{T}$ are computed based on the condition that the path forms a straight line in the space wrapping around the cylinder. To compute these coordinates, it is first necessary to compute the lengths of the path segments in the xy plane. The lengths of $\|\boldsymbol{PQ}\|_{xy}$ and $\|\boldsymbol{TS}\|_{xy}$ may be computed simply as the straight-line distance between the respective points. The length of line

segment $\|\boldsymbol{QT}\|_{xy}$ is found using the law of cosines, thus:

$$\|\boldsymbol{QT}\|_{xy} = \left| R\mathrm{Cos}^{-1}\left(1.0 - \frac{(Q_x - T_x)^2 + (Q_y - T_y)^2}{2R^2}\right)\right| \quad \text{(D.3)}$$

Knowing the lengths of the path segments in the xy plane, the z coordinates of $\boldsymbol{Q}$ and $\boldsymbol{T}$ may be found using similar triangle formulas, thus:

$$Q_z = P_z + \frac{(S_z - P_z)\|\boldsymbol{PQ}\|_{xy}}{\|\boldsymbol{PQ}\|_{xy} + \|\boldsymbol{QT}\|_{xy} + \|\boldsymbol{TS}\|_{xy}} \quad \text{(D.4)}$$

$$T_z = S_z - \frac{(S_z - P_z)\|\boldsymbol{TS}\|_{xy}}{\|\boldsymbol{PQ}\|_{xy} + \|\boldsymbol{QT}\|_{xy} + \|\boldsymbol{TS}\|_{xy}} \quad \text{(D.5)}$$

Determine Wrapping Conditions (Figure D, Step 3)

To determine whether or not $\boldsymbol{Q}$ and $\boldsymbol{T}$ are active, the wrapping conditions (see Appendix A) may be applied using the x and y coordinates of these points (Equation A.2):

$$\mathrm{Det} = (Q_x T_y - Q_y T_x) \Rightarrow \text{if } (R)(\mathrm{Det}) < 0, \text{ then wrapping does } \textit{not} \text{ occur} \quad \text{(D.6)}$$

Compute Muscle Segment Lengths (Figure D, Step 4)

If points $\boldsymbol{Q}$ and $\boldsymbol{T}$ are inactive, the minimum-distance path is simply a straight line between points $\boldsymbol{P}$ and $\boldsymbol{S}$. Otherwise, the minimum-distance path traverses from $\boldsymbol{P}$, through $\boldsymbol{Q}$, around the cylinder to $\boldsymbol{T}$, and terminates at $\boldsymbol{S}$. The lengths of segments $\boldsymbol{PQ}$ and $\boldsymbol{TS}$ may be computed simply as the straight-line distances between the respective points. Finally, the entire length of line segment $\boldsymbol{QT}$ may be found using equations D.3 to D.5, thus:

$$\|\boldsymbol{QT}\| = \sqrt{\|\boldsymbol{QT}\|_{xy}^2 + (T_z - Q_z)^2} \quad \text{(D.7)}$$

APPENDIX E — DOUBLE CYLINDER OBSTACLE-SET ALGORITHM

This version of the obstacle-set algorithm computes the minimum-distance path around a double cylinder obstacle set (see Figures E and 2C). The locations of the cylinder reference frame origins, $\boldsymbol{U}$ and $\boldsymbol{V}$, and the bounding fixed via points, $\boldsymbol{P}$ and $\boldsymbol{S}$, are known and are assumed to be expressed in the reference frame of the appropriate cylinder (Figure E, Step 1). The locations of the obstacle via points are computed by iteratively applying the single cylinder algorithm to the obstacle via points of each cylinder. Note that, for each cylinder, an obstacle via point on the opposite cylinder acts as a bounding-fixed via point, as expected by the single cylinder algorithm.

Reference Frames

U-Origin $\Rightarrow$ any convenient point along axis of the U-cylinder

U-Axes $\Rightarrow$ z-axis aligned with axis of U-cylinder, x- and y-axes orthonormal

V-Origin $\Rightarrow$ any convenient point along axis of the V-cylinder

V-Axes $\Rightarrow$ z-axis aligned with axis of V-cylinder, x- and y-axes orthonormal

Parameters

R_U $\Rightarrow$ radius of U-cylinder (positive or negative — see Appendix E)

R_V $\Rightarrow$ radius of V-cylinder (positive or negative — see Appendix E)

Inputs

$\boldsymbol{U}$ $\Rightarrow$ origin of U-cylinder frame expressed in V-cylinder frame

$\boldsymbol{V}$ $\Rightarrow$ origin of V-cylinder frame expressed in U-cylinder frame

$\boldsymbol{M}$ $\Rightarrow$ rotation matrix transforming points from U-cylinder to V-cylinder frame

$\boldsymbol{P}$ $\Rightarrow$ bounding fixed via point (in U-cylinder frame), start of path

$\boldsymbol{S}$ $\Rightarrow$ bounding fixed via point (in V-cylinder frame), end of path

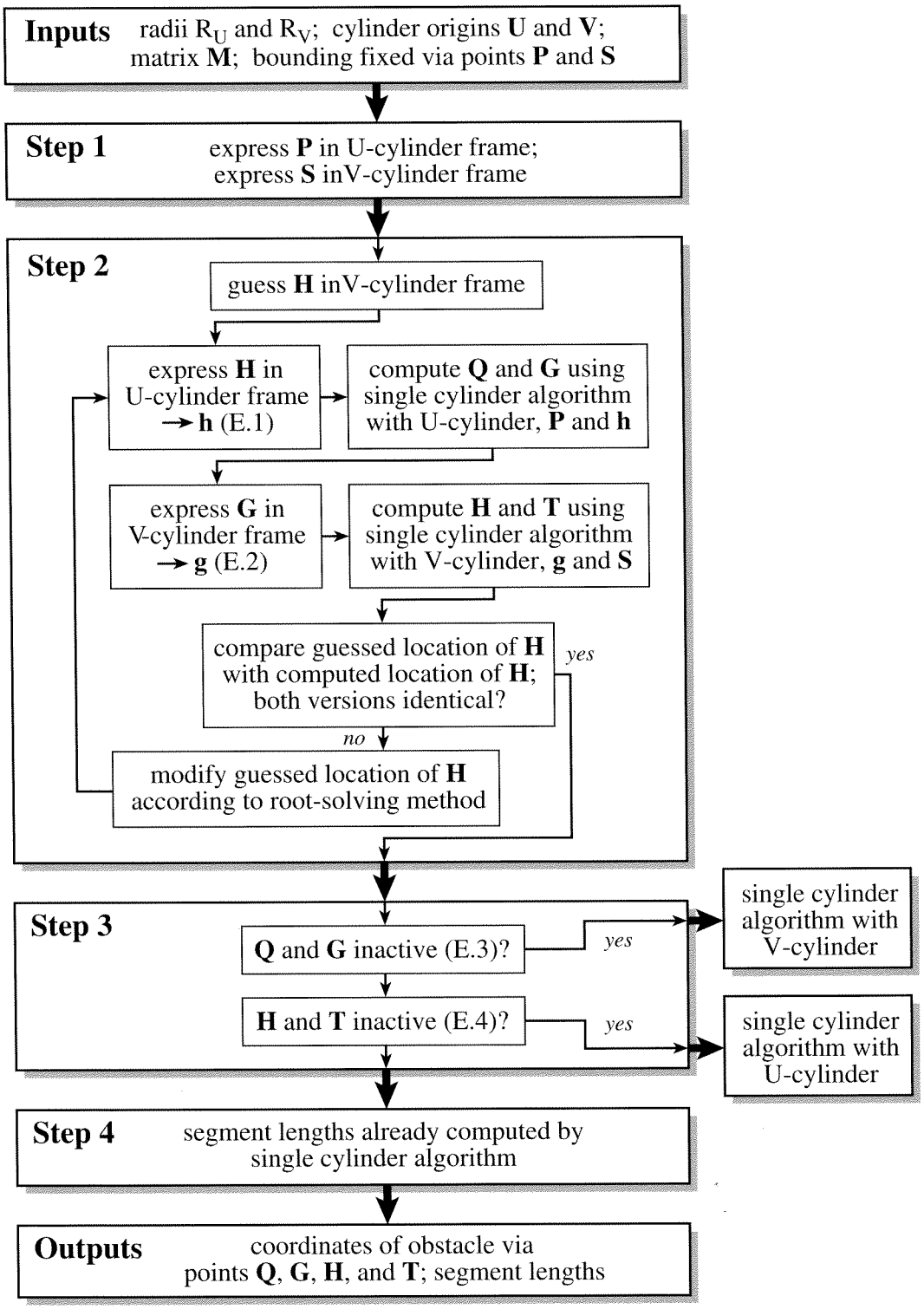

FIGURE E Flowchart of the double-cylinder obstacle-set algorithm. Symbols are defined in the text.

Outputs

$\boldsymbol{Q}$	$\Rightarrow$	obstacle via point (in U-cylinder frame), start of path which contacts U-cylinder
$\boldsymbol{G}$	$\Rightarrow$	obstacle via point (in U-cylinder frame), end of path which contacts U-cylinder
$\boldsymbol{H}$	$\Rightarrow$	obstacle via point (in V-cylinder frame), start of path which contacts V-cylinder
$\boldsymbol{T}$	$\Rightarrow$	obstacle via point (in V-cylinder frame), end of path which contacts V-cylinder
Lengths	$\Rightarrow$	lengths of path segments between points $\boldsymbol{P}$, $\boldsymbol{Q}$, $\boldsymbol{G}$, $\boldsymbol{H}$, $\boldsymbol{T}$, and $\boldsymbol{S}$

Compute Locations of Obstacle Via Points (Figure E, Step 2)

The double-cylinder obstacle set is treated as two single-cylinder obstacle sets except that the locations of the two inner obstacle via points ($\boldsymbol{G}$ and $\boldsymbol{H}$) are not independent. Specifically, the location of $\boldsymbol{H}$ on the V-cylinder affects the locations of $\boldsymbol{Q}$ and $\boldsymbol{G}$ on the U-cylinder, and the location of $\boldsymbol{G}$ on the U-cylinder affects the locations of $\boldsymbol{H}$ and $\boldsymbol{T}$ on the V-cylinder. Therefore, computing the locations of points $\boldsymbol{Q}$, $\boldsymbol{G}$, $\boldsymbol{H}$, and $\boldsymbol{T}$ requires an iterative approach. The approach we have adopted is as follows: 1) guess the location of $\boldsymbol{H}$; 2) compute the location of $\boldsymbol{Q}$ and $\boldsymbol{G}$ based on the initial guess; 3) compute the locations of $\boldsymbol{H}$ and $\boldsymbol{T}$ based on the location of $\boldsymbol{G}$; and 4) iteratively modify the guessed location of $\boldsymbol{H}$ until it matches the computed location of $\boldsymbol{H}$. Matching the x, y, and z coordinates of the guessed and computed locations of $\boldsymbol{H}$ forms three constraint equations which can be solved using standard root-solving techniques.

In order to compute the locations of $\boldsymbol{Q}$ and $\boldsymbol{G}$ based on the guessed location of $\boldsymbol{H}$ (step 2 above), the coordinates of $\boldsymbol{H}$ must be expressed in the U-cylinder frame (points expressed in the reference frame of the cylinder opposite their own will be written in lower case):

$$\boldsymbol{h} = \boldsymbol{V} + [\boldsymbol{M}]^T \boldsymbol{H} \tag{E.1}$$

The single cylinder algorithm can then be applied to the U-cylinder as if $\boldsymbol{h}$ were the second bounding-fixed via point (i.e; Appendix D is applied with $\boldsymbol{P}$ and $\boldsymbol{h}$ as inputs for the bounding-fixed via points, and $\boldsymbol{Q}$ and $\boldsymbol{G}$ as outputs for the obstacle via points).

The same process can be done in reverse to compute the locations of $\boldsymbol{T}$ and $\boldsymbol{H}$ based on that of $\boldsymbol{G}$ (step 3 above). First, the coordinates of $\boldsymbol{G}$ must be expressed in the V-cylinder frame:

$$\boldsymbol{g} = \boldsymbol{U} + [\boldsymbol{M}]\boldsymbol{G} \tag{E.2}$$

Then, the single cylinder algorithm can be applied to the V-cylinder as if $\boldsymbol{g}$ were the first of its bounding-fixed via points (i.e; Appendix D is applied with $\boldsymbol{g}$ and $\boldsymbol{S}$ as inputs for the bounding-fixed via points, and $\boldsymbol{H}$ and $\boldsymbol{T}$ as outputs for the obstacle via points).

Determine Wrapping Conditions (Figure E, Step 3)

To determine whether or not $\boldsymbol{Q}$ and $\boldsymbol{G}$ are active, and whether or not $\boldsymbol{H}$ and $\boldsymbol{T}$ are active, the wrapping conditions (see Appendix A) may be applied using x and y coordinates of these points (Equation A.2):

$$\text{Det} = (Q_x G_y - Q_y G_x) \Rightarrow \text{if } (R_U)(\text{Det}) < 0$$
$$\text{then path does } \textit{not} \text{ contact } U\text{-cylinder} \tag{E.3}$$

$$\text{Det} = (H_x T_y - H_y T_x) \Rightarrow \text{if } (R_V)(\text{Det}) < 0$$
$$\text{then path does } \textit{not} \text{ contact } V\text{-cylinder} \tag{E.4}$$

If the pair of obstacle via points associated with one of the cylinders proves to be inactive, the single cylinder algorithm should be applied to the other cylinder. The single cylinder algorithm may then show that the other cylinder is also inactive, in which case the minimum-distance path around the double-cylinder set is simply a straight line between $\boldsymbol{P}$ and $\boldsymbol{S}$.

Compute Muscle Segment Lengths (Figure E, Step 4)

If all the obstacle via points of the double-cylinder obstacle set are active, the minimum-distance path

traverses from ***P***, through ***Q***, around the U-cylinder to ***G***, across the gap between cylinders to ***H***, around the V-cylinder to ***T***, and finally terminates at ***S*** (see Figure 2C). The lengths of segments ***PQ***, ***GH***, and ***TS*** may be computed simply as the straight-line distances between the respective points. The lengths of segments ***QG*** and ***HT*** are calculated during iterations performed in steps 2 and 3 above.

APPENDIX F — SPHERE-CAPPED CYLINDER OBSTACLE-SET ALGORITHM

This version of the obstacle-set algorithm computes the minimum-distance path around a sphere-capped cylinder obstacle set (see Figures F and 2D). The locations of the origin of the sphere-capped reference frame, ***O***, and the bounding fixed via points, ***P*** and ***S***, are known and are assumed to be expressed in the sphere-capped cylinder reference frame (Figure F, Step 1). The locations of the obstacle via points, ***Q***, ***W***, and ***T***, are computed by methodically considering a number of possible configurations for the minimum-distance path (i.e; the path could contact only the cylinder section, only the sphere section, both the cylinder and sphere sections, or neither). If contact is found to occur on both the cylinder and sphere sections, the locations of the three obstacle via points are computed by an iterative process which attempts to simultaneously satisfy the minimum-distance conditions of both the sphere and the cylinder.

The sphere-capped cylinder algorithm further assumes a particular configuration for the bounding fixed via points. Specifically, the bounding-fixed via point at the start of the muscle path is assumed to be located more towards the cylinder section of the sphere-capped cylinder than the bounding fixed via point at the end of the muscle path (i.e; the z coordinate of ***P*** is assumed to be *less* than or *equal* to the z coordinate of ***S***). If the opposite happens to be true (i.e; the z coordinate of ***S*** is *greater* than the z coordinate of ***P***), then the algorithm should be applied with ***S*** as the starting point, ***P*** as the ending point, and the sign of the radius reversed (i.e; the algorithm should be applied with ***S***, ***P***, and -R, rather than ***P***, ***S***, and R, as inputs for the bounding fixed via points and radius, respectively).

Reference Frame

O ⇒ center of sphere, on axis of cylinder

Axes ⇒ z-axis aligned with axis of cylinder and positive towards sphere, x- and y-axes orthogonal. To avoid numerical problems, the x-axis should be positive towards area central to where most wrapping will occur.

Parameters

R ⇒ radius of sphere and cylinder (positive or negative — see Appendix B)

Inputs

P ⇒ bounding fixed via point, start of path

S ⇒ bounding fixed via point, end of path

Outputs

Q ⇒ obstacle via point, start of path which contacts the cylinder

W ⇒ obstacle via point, transition of path contact from cylinder to sphere

T ⇒ obstacle via point, end of path which contacts the sphere

Lengths ⇒ lengths of path segments between ***P***, ***Q***, ***W***, ***T***, and ***S***

Compute Locations of Obstacle Via Points (Figure F, Step 2)

To compute the locations of the obstacle via points, the various possible configurations of the minimum-distance path must be considered. Clearly, if ***P*** and ***S*** are both located towards either the cylinder or the sphere section, then the muscle path could only contact that section. Thus,

$$\text{if } (P_z \geq 0) \text{ and } (S_z \geq 0) \Rightarrow \text{path contacts only sphere, use single sphere algorithm} \quad \text{(F.1)}$$

$$\text{if } (P_z \leq 0) \text{ and } (S_z \leq 0) \Rightarrow \text{path contacts only cylinder, use single cylinder algorithm} \quad \text{(F.2)}$$

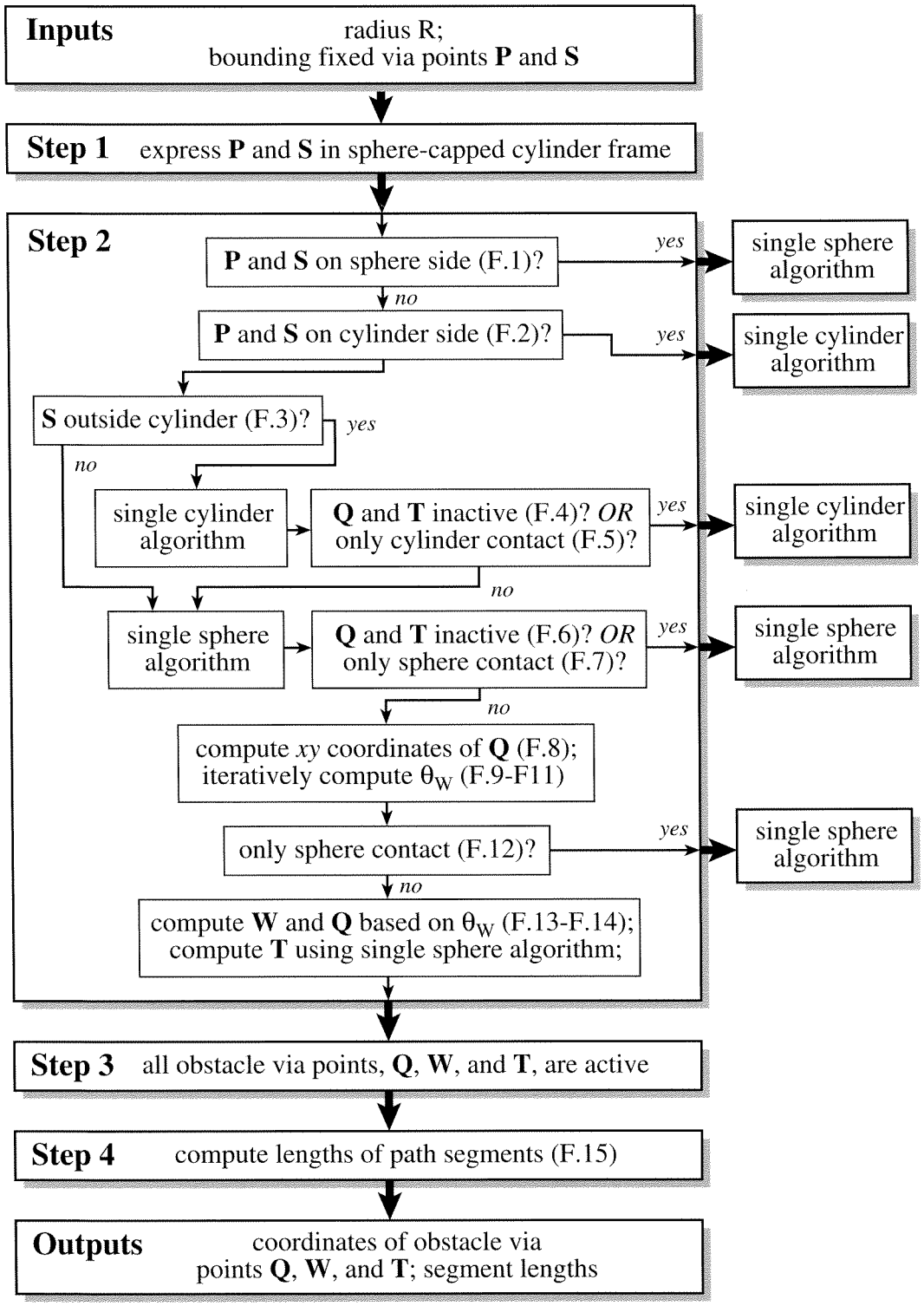

FIGURE F Flowchart of the sphere-capped cylinder obstacle-set algorithm. Symbols are defined in the text.

If neither of these sets of conditions is true, then $\boldsymbol{P}$ is located towards the cylinder section, and $\boldsymbol{S}$ is located towards the sphere section ($P_z < 0$ and $S_z > 0$). It is still possible, however, that the path contacts only the sphere or only the cylinder, in which case additional conditions must be checked. If $\boldsymbol{S}$ is located outside the volume of the cylinder (projected beyond the sphere), then the path may only contact the cylinder:

$$\text{if } (S_x^2 + S_y^2) \geq R^2 \Rightarrow \boldsymbol{S} \text{ is outside volume of cylinder, try single cylinder algorithm} \quad \text{(F.3)}$$

If condition (F.3) is true, the single cylinder algorithm should be tried. The results will reveal whether or not the path contacts only the cylinder. If the locations of $\boldsymbol{Q}$ and $\boldsymbol{T}$, computed by the single cylinder algorithm, are both towards the cylinder section, or if $\boldsymbol{Q}$ and $\boldsymbol{T}$ are found to be inactive, then the single cylinder algorithm results should be used, thus:

$$\text{if } \boldsymbol{Q} \text{ and } \boldsymbol{T} \text{ are inactive} \Rightarrow \text{path is a straight line, use single cylinder algorithm} \quad \text{(F.4)}$$

$$\text{if } (Q_z \leq 0) \text{ and } (T_z \leq 0) \Rightarrow \text{path contacts only cylinder, use single cylinder algorithm} \quad \text{(F.5)}$$

If condition (F.3) is not true, or if conditions (F.4) and (F.5) are not true, then the path may contact the sphere and possibly only the sphere. To check for these possibilities, the single sphere algorithm should be tried. The results will reveal whether or not the path contacts only the sphere. If the locations of $\boldsymbol{Q}$ and $\boldsymbol{T}$, computed by the single sphere algorithm, are both towards the sphere section, or if $\boldsymbol{Q}$ and $\boldsymbol{T}$ are found to be inactive, then the single sphere algorithm results should be used, thus:

$$\text{if } \boldsymbol{Q} \text{ and } \boldsymbol{T} \text{ are inactive} \Rightarrow \text{path is a straight line, use single sphere algorithm} \quad \text{(F.6)}$$

$$\text{if } (Q_z \leq 0) \text{ and } (T_z \leq 0) \Rightarrow \text{path contacts only sphere, use single sphere algorithm} \quad \text{(F.7)}$$

If conditions (F.6) and (F.7) are not true, then the path is assumed to contact both the cylinder and the sphere. In this case, by the definitions of the respective obstacle via points, $\boldsymbol{Q}$ will be on the surface of the cylinder, $\boldsymbol{W}$ will be on the seam joining the cylinder and the sphere ($W_z = 0$), and $\boldsymbol{T}$ will be on the surface of the sphere. The problem is then to compute the locations of these points which satisfy the criterion for a minimum-distance path around both the cylinder and sphere. As in the single cylinder algorithm, the x and y coordinates of $\boldsymbol{Q}$ may be computed based on the circle tangency equations (see Appendices B and C):

$$Q_x = \frac{P_x R^2 + R P_y \sqrt{P_x^2 + P_y^2 - R^2}}{(P_x^2 + P_y^2)}$$
$$Q_y = \frac{P_y R^2 - R P_x \sqrt{P_x^2 + P_y^2 - R^2}}{(P_x^2 + P_y^2)} \quad \text{(F.8)}$$

Further, as in the single sphere algorithm, the location of $\boldsymbol{W}$ can be computed based on the locations of $\boldsymbol{S}$ and $\boldsymbol{Q}$ (independent of the location of $\boldsymbol{T}$). Conveniently, since the location of $\boldsymbol{P}$ is known, the z coordinate of $\boldsymbol{Q}$ is not needed in order to compute $\boldsymbol{W}$. In fact, it can be shown that the following equation is a necessary condition for the minimum-distance path criterion:

$$\left[-P_z \sqrt{S_x^2 + S_y^2}\right] \sin(\theta_W - \theta_S) + [S_z |R|](\theta_W - \theta_Q) + \left[S_z \sqrt{(P_x - Q_x)^2 + (P_y - Q_y)^2}\right] \frac{R}{|R|} = 0 \quad \text{(F.9)}$$

where θ_W, θ_S, θ_Q, and θ_P are the trigonometric angles formed by the x and y coordinates of via points $\boldsymbol{W}$, $\boldsymbol{S}$, $\boldsymbol{Q}$, and $\boldsymbol{P}$, respectively:

$$\theta_W \equiv \text{Tan}^{-1}\left(\frac{W_y}{W_x}\right) \quad \theta_S \equiv \text{Tan}^{-1}\left(\frac{S_y}{S_x}\right)$$
$$\theta_Q \equiv \text{Tan}^{-1}\left(\frac{Q_y}{Q_x}\right) \quad \theta_P \equiv \text{Tan}^{-1}\left(\frac{P_y}{P_x}\right) \quad \text{(F.10)}$$

The only unknown in Equation (F.9) is the value of θ_W, which can be found using standard root-solving techniques. Because the valid solution for θ_W in Equation (F.9) must lie between θ_P and θ_S (θ_W

lies between θ_P and θ_S in the path), a good initial guess for the root solver can be made by linearly interpolating between the angles, thus:

$$\theta_W(\text{guess}) = \theta_P - (\theta_S - \theta_P)\frac{P_z}{S_z - P_z} \qquad \text{(F.11)}$$

Once Equation (F.9) has been satisfied, the computed value of θ_W should be compared with the value of θ_Q, because θ_Q should come before θ_W in the path. If the values are reversed in order (according to the wrapping direction), then the path must, after all, contact only the sphere:

$$\text{if } (R > 0) \text{ and } (\theta_W \leq \theta_Q) \Rightarrow \text{ path contacts only sphere, use single sphere algorithm} \qquad \text{(F.12a)}$$

$$\text{if } (R < 0) \text{ and } (\theta_W \geq \theta_Q) \Rightarrow \text{path contacts only sphere, use single sphere algorithm} \qquad \text{(F.12b)}$$

If neither of conditions (F.12) is true, the minimum-distance path contacts both the cylinder and the sphere. The remaining unknown components of $\boldsymbol{W}$ and $\boldsymbol{Q}$ may be then computed:

$$W_x = |R|\cos(\theta_W) \quad W_y = |R|\sin(\theta_W)$$
$$W_z = 0 \qquad \text{(F.13)}$$

$$Q_z = W_z + \frac{|R(\theta_W - \theta_Q)|P_z}{|R(\theta_W - \theta_Q)| + \|\overline{\boldsymbol{PQ}}\|_{xy}} \qquad \text{(F.14)}$$

Finally, the location of $\boldsymbol{T}$ may be computed by applying with single sphere algorithm with $\boldsymbol{W}$ and $\boldsymbol{S}$ used as inputs for the bounding fixed via points.

Determine Wrapping Conditions (Figure F, Step 3)

The process of computing the locations of the obstacle via points for the sphere-capped cylinder obstacle set have already determined what wrapping configuration the minimum-distance path will take. Therefore, no additional conditions need to be checked.

Compute Muscle Segment Lengths (Figure F, Step 5)

Assuming that the minimum-distance path contacts both the cylinder and the sphere, all three via points, $\boldsymbol{Q}$, $\boldsymbol{W}$, and $\boldsymbol{T}$, will be active. The path therefore traverses from $\boldsymbol{P}$, through $\boldsymbol{Q}$, around the cylinder to $\boldsymbol{W}$, around the sphere to $\boldsymbol{T}$, and finally terminates at $\boldsymbol{S}$ (see Figure 2D). The lengths of segments $\boldsymbol{PQ}$ and $\boldsymbol{TS}$ may be computed simply as the straight-line distances between the respective points. The length of segment $\boldsymbol{WT}$ will have been computed by the single sphere algorithm used to compute the location of $\boldsymbol{T}$. Finally, the length of segment $\boldsymbol{QW}$ may be computed based on the arc length:

$$\|\boldsymbol{QW}\| = \sqrt{(R(\theta_W - \theta_Q))^2 + (T_z - Q_z)^2} \qquad \text{(F.15)}$$

Acknowledgments

Partial funding for this work was provided by NASA Grants NGT-51025 and NAG9-805. We thank the National Library of Medicine for making available to us the Visible Human Project dataset. Support provided by the Visualization Laboratory at The University of Texas Center for High Performance Computing is also gratefully acknowledged.

References

[1] Paul, J. P. (1965). Bioengineering studies of the forces transmitted by joints: II. Engineering analysis. In Kenedi, R. M. (ed.): Biomechanics and Related Bioengineering Topics, Pergamon Press, Oxford.

[2] Morrison, J. B. (1970). The mechanics of the knee joint in relation to normal walking. *Journal of Biomechanics*, **3**, 51–61.

[3] Seireg, A. and Arvikar, R. J. (1975). The prediction of muscular load sharing and joint forces in the lower extremities during walking. *Journal of Biomechanics*, **8**, 89–102.

[4] Hatze, H. (1976). The complete optimization of human motion. *Mathematical Biosciences*, **28**, 99–135.

[5] Hardt, D. E. (1978). Determining muscle forces in the leg during normal human walking — An application and evaluation of optimization methods. *Journal of Biomechanical Engineering*, **100**, 72–78.

[6] Amis, A. A., Dowson, D. and Wright, V. (1980). Elbow joint force predictions for some strenuous isometric actions. *Journal of Biomechanics*, **13**, 765–775.

[7] Patriarco, A. B., Mann, R. W., Simon, S. R. and Mansour, J. M. (1981). An evaluation of the approaches of optimization methods in the prediction of muscle forces during human gait. *Journal of Biomechanics*, **14**, 513–525.

[8] Davy, D. T. and Audu, M. L. (1987). A dynamic optimization technique for predicting muscle forces in the swing phase of gait. *Journal of Biomechanics*, **20**, 187–201.
[9] Karlsson, D. and Peterson, B. (1992). Towards a model for force predictions in the human shoulder. *Journal of Biomechanics*, **25**, 189–192.
[10] Buchanan, T. S., Moniz, M. J., Dewald, J. P. and Rymer, W. Z. (1993). Estimation of muscle forces about the wrist joint during isometric tasks using an EMG coefficient method. *Journal of Biomechanics*, **26**, 547–560.
[11] Collins, J. J. (1995). The redundant nature of locomotor optimization laws. *Journal of Biomechanics*, **28**, 251–267.
[12] Pandy, M. G. and Shelburne, K. B. (1997). Dependence of cruciate-ligament loading on muscle forces and external load. *Journal of Biomechanics*, **30**, 1015–1024.
[13] Pandy, M. G., Sasaki, K. and Kim, S. (1998). A three-dimensional musculoskeletal model of the human knee joint. Part I: Theoretical construction. *Computer Methods in Biomechanics and Biomedical Engineering*, **1**, 87–108.
[14] Anderson, F. C. and Pandy, M. G. (in press). A dynamic optimization solution for vertical jumping in three dimensions. *Computer Methods in Biomechanics and Biomedical Engineering*.
[15] Herzog, W. (1992). Sensitivity of muscle force estimation to changes in muscle input parameters using nonlinear optimization. *Journal of Biomechanical Engineering*, **114**, 267–268.
[16] Brand, R. A., Pedersen, D. R., Davy, D. T., Kotzar, G. M., Heiple, K. G. and Goldberg, V. M. (1994). Comparison of hip force calculations and measurements in the same patient. *Journal of Arthroplasty*, **9**, 45–51.
[17] Seireg, A. and Arvikar, R. J. (1973). A mathematical model for evaluation of forces in the lower extremities of the musculoskeletal system. *Journal of Biomechanics*, **6**, 313–326.
[18] Crowninshield, R. D., Johnston, R. C., Andrews, J. G. and Brand, R. A. (1978). A biomechanical investigation of the human hip. *Journal of Biomechanics*, **11**, 75–85.
[19] Dostal, W. F. and Andrews, J. G. (1981). A three-dimensional biomechanical model of hip musculature. *Journal of Biomechanics*, **14**, 803–812.
[20] Brand, R. A., Crowninshield, R. D., Wittstock, C. E., Pedersen, D. R., Clark, C. R. and van Krieken, F. M. (1982). A model of lower extremity muscular anatomy. *Journal of Biomechanical Engineering*, **104**, 304–310.
[21] Jensen, R. H. and Davy, D. T. (1975). An investigation of muscle lines of action about the hip: A centroid line approach vs the straight line approach. *Journal of Biomechanics*, **8**, 103–110.
[22] Bassett, R. W., Browne, A. O., Morrey, B. F. and An, K. N. (1990). Glenohumeral muscle force and moment mechanics in a position of shoulder instability. *Journal of Biomechanics*, **23**, 405–415.
[23] Tsuang, Y. H., Novak, G. J., Schipplein, O. D., Hafezi, A., Trafimow, J. H. and Anderson, G. B. (1993). Trunk muscle geometry and centroid location when twisting. *Journal of Biomechanics*, **26**, 537–546.
[24] An, K. N., Hui, F. C., Morrey, B. F., Linscheid, R. L. and Chao, E. Y. (1981). Muscles across the elbow joint: A biomechanical analysis. *Journal of Biomechanics*, **14**, 659–669.
[25] An, K. N., Takahashi, K., Harrigan, T. P. and Chao, E. Y. (1984). Determination of muscle orientations and moment arms. *Journal of Biomechanical Engineering*, **106**, 280–282.
[26] Wood, J. E., Meek, S. G. and Jacobsen, S. C. (1989). Quantitation of human shoulder anatomy for prosthetic arm control — II. Anatomy matrices. *Journal of Biomechanics*, **22**, 309–325.
[27] Delp, S. L., Loan, J. P., Hoy, M. G., Zajac, F. E., Topp, E. L. and Rosen, J. M. (1990). An interactive graphics-based model of the lower extremity to study orthopedic surgical procedures. *IEEE Transactions on Biomedical Engineering*, **37**, 757–767.
[28] Yoon, I. and Thompson, D. E. (1990). Planning tendon paths using an interactive graphic workstation. *Journal of Biomechanical Engineering*, **112**, 387–391.
[29] Winters, J. M. and Kleweno, D. G. (1993). Effect of initial upper-limb alignment on muscle contributions to isometric strength curves. *Journal of Biomechanics*, **26**, 143–153.
[30] Pierrynowski, M. R. (1995). Analytic representation of muscle line of action and geometry. In Allard, P., Stokes, I. A. F., Blanchi, J.-P. (eds.): Three-dimensional Analysis of Human Movement. Human Kinetics, Champaign, IL, pp. 214–256.
[31] Shelburne, K. B. and Pandy, M. G. (1997). A musculoskeletal model of the knee for evaluating ligament forces during isometric contractions. *Journal of Biomechanics*, **30**, 163–176.
[32] Hogfors, C., Sigholm, G. and Herberts, P. (1987). Biomechanical model of the human shoulder — I. Elements. *Journal of Biomechanics*, **20**, 157–166.
[33] van der Helm, F. C., Veeger, H. E., Pronk, G. M., van der Woude, L. H. and Rozendal, R. H. (1992). Geometry parameters for musculoskeletal modelling of the shoulder system. *Journal of Biomechanics*, **25**, 129–144.
[34] Garner, B. A. and Pandy, M. G. (in press). A kinematic model of the upper limb based on the Visible Human Project (VHP) dataset. *Computer Methods in Biomechanics and Biomedical Engineering*.
[35] Otis, J. C., Jiang, C. C., Wickiewicz, T. L., Peterson, M. G., Warren, R. F. and Santner, T. J. (1994). Changes in the moment arms of the rotator cuff and deltoid muscles with abduction and adduction. *Journal of Bone and Joint Surgery*, **76-A**, 667–676.
[36] Murray, W. M., Delp, S. L. and Buchanan, T. S. (1995). Variation of muscle moment arms with elbow and forearm position. *Journal of Biomechanics*, **28**, 513–525.
[37] Brand, P. W., Cranor, K. C. and Ellis, J. C. (1975). Tendon and pulleys at the metacarpophalangeal joint of a finger. *Journal of Bone and Joint Surgery*, **57A**, 779–784.
[38] An, K. N., Ueba, Y., Chao, E. Y., Cooney, W. P. and Linschied, R. L. (1983). Tendon excursion and moment arm of index finger muscles. *Journal of Biomechanics*, **16**, 419–425.
[39] Spoor, C. S., van Leeuwen, J. L., Meskers, C. G., Titulaer, A. F. and Huson, A. (1990). Estimation of instantaneous moment arms of lower-leg muscles. *Journal of Biomechanics*, **23**, 1247–1259.
[40] Lemay, M. A. and Crago, P. E. (1996). A dynamic model for simulating movements of the elbow, forearm, and wrist. *Journal of Biomechanics*, **29**, 1319–1330.
[41] van der Helm, F. C. and Veenbaas, R. (1991). Modelling the mechanical effect of muscles with large attachment sites: Application to the shoulder mechanism. *Journal of Biomechanics*, **24**, 1151–1163.
[42] Dostal, W. F., Soderburg, G. L. and Andrews, J. G. (1986). Actions of hip muscles. *Physical Therapy*, **66**, 351–361.
[43] Pandy, M. G. (1999). Moment arm of a muscle force. In Holloszy, J. O. (ed.): *Exercise and Sport Sciences Reviews*, Williams and Wilkins, Baltimore, MD, **27**, pp. 79–118.